A Theoretical Study of Cr/oxide Catalysts for Dehydrogenation of Short Alkanes

Sindre Lillehaug

Department of Chemistry
University of Bergen
2006

Dissertation submitted for the degree of *doctor scientiarum*

Jeg skjønner alt for mye og ingenting
Og hjernen min sier pling pling pling [a]

[a] Lars Lillo-Stenberg

Preface

Natural gas reserves are being produced at increasing rates world wide, thus providing an abundance of short-alkane feedstock for the petrochemical industry. Effective routes to selective activation of short alkanes may represent a bottleneck of this development. In this respect, processes of catalytic dehydrogenation have significant economic potential. Several catalysts have been investigated and some are implemented industrially. At the core of one such catalyst are species of chromium oxide supported on the surface of amorphous alumina. Since the original report by Frey and Huppke in 1933, this system has been under study, the literature expanding with the development of experimental methods. However, due to the heterogeneity of the Cr/alumina surfaces a structure-activity relationship has not been determined to date. Opinions are converging regarding the oxidation state of active chromium, but little is known about the nano-range surroundings of the active site. The involvement of oxygen ligands is a popular issue related to the mechanism of catalysis. Other remaining questions concern the chromium nuclearity of the active surface site and the role of the oxide support.

With the development of quantum chemical tools and powerful hardware, computational modelling emerges as a manageable complement to experiment. The combination may lead to novel insight into the structure-activity relationship on Cr/oxide surfaces. Ultimately this may contribute to more effective catalysts by rational design.

For this thesis, model catalysts have been investigated computationally with respect to (i) mechanisms of catalytic dehydrogenation, and (ii) surface reactions of chromium precursor species leading to the active catalyst. The work includes simulated annealing to generate realistic surface models, and reactivity studies based on cluster and embedded-cluster approaches. Based on these computations, two mechanisms of catalytic dehydrogenation appear viable depending on the nano range surrounding the active site. One mechanism is found to involve cleavage and reformation of a Cr–O bond. However, the activation energy of this mechanism is found prohibitively high unless the Cr–O bond is weakened by structural strain. Alternatively, a pre-catalytic step of C–H activation in alkane involving irreversible cleavage of a Cr–O bond is found leading to formation of a hydridochromium moiety, which appears highly active according to a second mechanism of catalytic dehydrogenation. Regarding the role of the support, this is proposed one of providing precursor species and sustaining the reactive sites. Moreover, it appears that polynuclear sites of the active chromium species are formed in the typical steps of catalyst preparation. These results form the basis for a hypothesis on which novel experiments are suggested.

Acknowledgements

I would like to thank my supervisor Prof. Knut J. Børve. Patiently and with apparent unlimited knowledge, he has guided me through an interesting period of learning. Furthermore, Dr. Vidar R. Jensen has acted as a second supervisor, always having time for a chat on subjects of chemistry or other. I am also indebted to Prof. Joachim Sauer and Dr. Marek Sierka for their hospitality and help during my stay at the Humboldt University in Berlin. Prof. Rolf Manne and my father are thanked for their assistance in the preparation of this thesis. Thanks are also in order for my fellow students here at the university of Bergen. In particular, the help by Manuel Sparta is much appreciated. It is also important to mention the group of mountain bikers who have had a vital role in maintaining my sanity throughout this work.

Most of all, I am indebted to my family for unlimited support, and to Raquel for her incredible patience.

Funding for this research has been provided by the Research Council of Norway, computer time being awarded through the Programme for Supercomputing.

Bergen, April 2006
Sindre Lillehaug

Contents

List of Papers

This thesis is based on the following scientific papers.

I Catalytic Dehydrogenation of Ethane over Mononuclear Cr(III)/silica Surface Sites. Part I. C–H Activation by σ-bond Metathesis.
Sindre Lillehaug, Knut J. Børve, Marek Sierka and Joachim Sauer.
Journal of Physical Organic Chemistry **17**, 990-1006 (2004).

II Catalytic Dehydrogenation of Ethane over Mononuclear Cr(III)/silica Surface Sites. Part II. C-H Activation by Oxidative Addition.
Sindre Lillehaug, Vidar R. Jensen and Knut J. Børve.
Journal of Physical Organic Chemistry **19**, 25-33 (2006).

III The Role of the Carrier Oxide in Cr/oxide Catalysts for Dehydrogenation of Ethane.
Sindre Lillehaug and Knut J. Børve. (Manuscript)

IV Oxidation of Cr(II) to Cr(III) on the Surface of Amorphous Silica, with Implications for Catalytic Dehydrogenation of Ethane.
Sindre Lillehaug and Knut J. Børve. (Manuscript)

Chapter 1

Introduction

In the first decades of the twentieth century, the demand for refined petroleum products soared as the consequence of a successful automobile industry. The demand was met by development of processes for refining of crude oil by cracking, which in addition to the petroleum main product yield large quantities of gaseous hydrocarbons. Though initially considered waste products, usable only as fuels, these hydrocarbons now feed the vast industry of petrochemistry. After a childhood period spent in laboratories, the petrochemical industry broke into adolescence in the 1930s with the commercial manufacture of polymer materials such as PVC and nylon. World war II then brought a time of shortages, spurring an escalation in the production of synthetic materials including plastics, fibres, rubbers, and teflon. These were prioritized to military uses during the war, but subsequently applied in numerous household articles, pushing the industry to maturity by 1970 [1].

Today, the products of the petrochemical industry are inescapable, and a large fraction of the feedstock is C2-C4 alkanes; ethane, propane and butanes. Propane and butanes are the main components of Liquid Petroleum Gas (LPG), which is obtained from the cracking of heavy hydrocarbons. In addition, the C2-C4 alkanes constitute various proportions of Natural Gas Liquid (NGL), which is separated from methane in the processing of natural gas. Thus, with increasing focus on natural gas as an energy source, vast supplies of feedstock are becoming available for the petrochemical industry.

1.1 Dehydrogenation of Short Alkanes

Alkanes are readily reacted to yield carbon oxides and water under release of energy, hence the extended use as fuels. For selective activation, on the other hand, partial oxidation is necessary, and the task becomes increasingly difficult with the stronger C–H bonds of shorter alkanes. The challenge of this task, together with the economic incentive, has spurred widespread research activity in academic circles, where controlled C–H activation has been considered a "holy grail" [2].

One common route to partial oxidation of alkanes is by dehydrogenation to alkenes, also called olefins. In the process, a H_2 molecule is removed according to the general reaction:

$$C_nH_{2n+2} \rightarrow C_nH_{2n} + H_2$$

Reflecting the strength of the C–H bonds broken in the reaction, the thermodynamics are unfavourable. For instance, 50% conversion of propane requires a reaction temperature of 595°C, and the same conversion of ethane requires a temperature of 725°C [3]. However, the expense is justified by the specific reactivity of the carbon-carbon double bond in the resulting olefin. This is effectively exploited in catalytic polymerization, the main use of olefins is therefore in the manufacture of plastics and rubbers. Examples of other uses are as building blocks for gasoline, and in the ripening of fruit.

In addition to olefins, the other major product of dehydrogenation is molecular hydrogen, H_2, which as a clean source of energy represents an additional economic and ecologic incentive for the process [4].

Olefins have typically been obtained by non-catalytic steam cracking of light alkanes, and as by-products from the cracking of heavy hydrocarbons in the manufacture of gasoline [5]. These processes are flexible with regard to feedstock, which may be chosen depending on price and availability. However, the production of olefins as by-products renders the supply unflexible with respect to the demand. Furthermore, selectivity is a problem of steam cracking. The reaction yields both diolefins and acetylene, which are separated from the product stream and catalytically hydrogenated to olefins. Thus, with increasing demand for specific olefins such as isobutene and propene, and increasing availability of light alkanes from natural gas, there is a market for efficient and selective processes of dehydrogenation. This brings us to the present topic of catalytic dehydrogenation.

Catalytic Dehydrogenation of Short Alkanes The function of a catalyst is to increase the reaction rate by providing an alternative, less energy-demanding path to products, without itself being consumed in the process. Contrary to the cracking processes, which are based on gas-phase free-radical reactions, the products of dehydrogenation are formed during contact of the reacting alkane with the catalyst. The activity is typically centered at a transition metal complex or a small transition metal cluster. Known catalysts for dehydrogenation fall into groups of molecular transition metal complexes [6] and surface catalysts including finely dispersed platinum [7–9] and Cr/oxide [3]. Industrial applications are based on chromia or platina dispersed on alumina [10]. These are heterogeneous catalysts in the sense that the reaction takes place at the interphase between the gas phase and the solid catalyst. The selectivity to dehydrogenation is close to 90%, though, for dehydrogenation of, e.g., propane and butanes, the limitations of thermodynamics render a per-pass conversion in the range of 30-60% [3, 10].

Cr/alumina catalysts were first used in the late 1930s in the production of butenes, which were subsequently dimerized to give high-octane aviation fuel. N-butane remained the main reactant of catalytic dehydrogenation until the late 1980s, when large quantities of butadiene had become available as a by-product from cracking of naphtha and other heavy hydrocarbons. The industry then shifted to dehydrogenation of propane, for the polymer industry, and dehydrogenation of iso-butane in the production of methyl tertiary

butyl ether (MTBE), which added to gasoline increases the octane rating. For a historical and current account of industrial processes for catalytic dehydrogenation see the recent report by Bhasin *et al.* [10].

1.2 Cr/oxide Catalysts for Alkane Dehydrogenation

The catalytic dehydrogenation of C2-C4 alkanes over a Cr/alumina surface was first reported in 1933 by Frey and Huppke [11]. Since then, the catalyst has been under study and the catalytic performance has been tuned with respect to activity, selectivity, and lifetime on stream [3, 12]. The approach has been one of classical catalyst design, i. e. optimization by variation of the parameters of catalyst composition and preparation. As the consequence of these studies, current industrial applications use 13 wt% Cr/alumina, and a dopant consisting of alkali metal to minimize coking and thus extending the lifetime on stream [3, 13]. Further enhancement of catalyst performance has been sought through more rational design, the first step being to determine the structure of the active chromium surface species. However, this is a difficult task due to the heterogeneity of Cr/oxide surfaces. To cope with this problem, variety of experimental designs have been made, combining complemental techniques of characterization with tests of catalytic activity and selectivity. Key parameters of all these studies are the catalyst composition and the steps of catalyst preparation.

Catalyst Composition In attempts to relate chromium speciation and catalytic activity, the generic 0-20 wt% Cr/oxide system, as well as unsupported α-chromia, has been studied. Chromium is found active in the entire 0-20 weight-percent range on alumina support, which is used for industrial applications, but also on silica, zirconia, titania [3]. Even crystalline α-chromia is reported to be active in catalytic dehydrogenation [14–17], though less than the dispersed phase [18].

Below 2 wt% chromium on alumina, silica and zirconia, the catalytic activity increases linearly with the chromium load, and has been interpreted in terms of mononuclear active species [3, 17, 19–21]. On the other hand, the high activity of Cr/alumina at chromium load exceeding monolayer coverage indicates active sites also on species of polynuclear chromium(III) [18, 22–25].

The relative catalytic activity depending on oxide carrier has been reported as Cr/zirconia > Cr/alumina > Cr/silica > α-chromia [17, 20, 26–28]. However, DeRossi *et al.* [17] reported similar activation energies for the catalytic dehydrogenation over Cr/alumina, Cr/silica and chromia. Furthermore, the observation by Lugo and Lunsford [16] of similar turnover frequency per chromium atom on alumina and silica has been interpreted in terms of similar active species on these supports [16, 18]. Actually, there appears to be a generally consensus in the literature that differences in activity depending on the support stem from the ability to stabilize the active species. In particular, the nature of the active species has often been investigated by study of catalytic activity with respect to variation in chromium surface structures on alumina and silica supports, e. g., see Refs. [16, 17, 26, 27]. The higher covalency of silica relative to alumina [29]

causes differences chromium speciation. In short, the dispersion of chromium is better on alumina [20,30,31], which stabilizes mainly Cr(III) during reaction conditions [21,32,33], whereas on silica the ratio of Cr(II) and Cr(III) may be tuned by varying details of the catalyst preparation [17, 34] (*vide infra*). Somewhat higher activity of Cr/alumina relative to Cr/silica has thus been ascribed to the stabilization of dispersed amorphous Cr(III) species [27]. Further insight has been obtained by experimental design combining variations in the catalyst composition and preparation.

Catalyst Preparation The chromium species that are active in catalytic dehydrogenation have typically been investigated by characterization of the surface species that are formed in each step of the preparation. Usually, a chromium precursor is added to the oxide carrier in aqueous medium, which is subsequently evaporated. The dried catalyst is then calcined by heating in oxygen-rich environment at elevated temperatures, and finally, the active chromium species are formed by reduction [3].

Calcination leaves dispersed chromium ions mainly in the +VI state, while minor amounts are found in the +V state [35]. The dispersion of chromium comes through interaction with surface hydroxyl groups on the hydrated support [36–38], and calcination yields anchoring in the form of Cr–O–M links, M=Al and M=Si on alumina and silica, respectively [18,27,39–43]. Higher population and basicity of surface hydroxyls on alumina than on silica results in better dispersion of chromium on alumina [30]. In fact, the surface of silica appears to facilitate the aggregation chromium in crystalline α-Cr_2O_3 particles [30,31,44].

Before becoming active in catalytic dehydrogenation, the calcined surface of Cr/oxide must be reduced, typical reducing reagents being H_2, CO, or the alkane feed [17,25,33,45–48]. IR and Raman spectra show that during reduction the oxo ligands of dispersed Cr(VI) species are consumed [42, 49]. However, illustrative of the complexity of the Cr/oxide surfaces, there has been a long standing controversy concerning the active oxidation state of chromium. Both Cr(II) [16,50] and Cr(III) [14,15,51] were proposed quite early.

The Oxidation State of Active Chromium In attempts to resolve the issue of the active oxidation state, workers in the field have exploited the different redox properties of chromium when anchored on silica and on alumina. For instance, reduction of the calcined surface with CO gives mainly Cr(II) and mainly Cr(III) on silica and alumina, respectively. On mixed silica-alumina supports, Weckhuysen *et al.* [26] observed a linear increase in activity with the amount of pseudo-octahedral Cr(III), which correlates with the alumina content. Conversely, in a study of Cr/silica, DeRossi *et al.* [17] selectively oxidized Cr(II) to Cr(III) by heating with water, and the subsequent catalytic activity was taken as proof of active Cr(III). While these results show that Cr(III) species are most likely active in catalytic dehydrogenation of alkanes on both silica and alumina supports, a contribution from Cr(II)/silica has not been ruled out. While Lugo and Lunsford [16] ascribed all activity on the CO-reduced Cr/silica to Cr(II), Hakuli *et al.* [52] found Cr(II) active, though less than Cr(III). A common observation in these studies is that isolated species of Cr(II) on silica are quickly deactivated by coking [16,52].

In summary of modern literature, the dominant view is that +III is the most active oxidation state for dehydrogenation, possibly with minor contributions from +II [17, 18, 21, 26, 52, 53].

The Active Cr(III) Species Below monolayer coverage of chromium on alumina, silica and zirconia, a linear relationship has been found between the number of mononuclear Cr(V) and Cr(VI) species on the calcined surface, and the catalytic activity after reduction to Cr(III) [17, 20, 22, 54, 55]. A candidate for the active species is therefore *redox Cr(III)*, described as Cr(III) species resulting from the reduction of high-valent chromium [17, 19–21, 26, 56, 57]. Moreover, mononuclear redox Cr(III) species have been proposed based on the linear increase in activity with chromium loading below 2 wt% [3,17,19–21]. However, through preparation of Cr/oxide catalysts by Atomic Layer Epitaxy (ALE), the calcination step of the catalyst preparation may be omitted. In this way, catalytically active species of Cr(III) have been formed without passing chromium through the high-valent state [25]. These species, described as *non-redox Cr(III)*, have been associated with amorphous chromia dispersed on the oxide support, and have been attributed high activity in catalytic dehydrogenation [18, 22–25].

It appears that two types of Cr(III) surface species may be active in catalytic dehydrogenation on Cr/oxide catalysts; redox- and non-redox Cr(III), or, alternatively, that the activity of a Cr(III) ion is determined by its environment rather than redox history [25]. Moreover, Cavani *et al.* [18] summarize from the literature that activity generally appears to be a function of chromium coverage, rather than initial state and aggregation.

To characterize the local environment of the active Cr(III) species, Weckhuysen *et al.* [26] applied *in situ* diffuse-reflectance UV-vis spectroscopy (DRS) on Cr/alumina and established a semi-quantitative relationship between the number of pseudo-octahedral Cr(III) sites and dehydrogenation activity. Further clues are provided by infra-red spectroscopy studies of CO and NO adsorbed onto reduced Cr species on silica [17] and zirconia [58]. Together with measurements of dehydrogenation activity, these experiments led to the conclusion that the most active Cr(III) has two coordinative vacancies. From its spectroscopic signature, this species was called Cr(III)G, and DeRossi *et al.* [17] went on to propose a possible structure in which a chromiumhydroxyl is bonded to the oxide surface by two oxygen bridges, cf. Fig. 1.1.

1.3 Model-Based Study of the Cr/alumina Catalyst

The study of surface species and reactions on a Cr/oxide catalyst is difficult due to the heterogeneity of the surfaces. Therefore, to elucidate the activity of different chromium species in catalytic dehydrogenation, the generic Cr/oxide system has typically been applied with varying chromium load, to model the 13 wt% Cr/alumina catalyst in industrial applications (*vide supra*). Furthermore, to simplify the set of catalytic reactions, ethane has been studied as reactant alkane in place of propane or butanes [14–16, 59].

The present computational study is model based in its entirety. This includes the tools of computational chemistry, as well as the combinations of Cr/oxide surface species

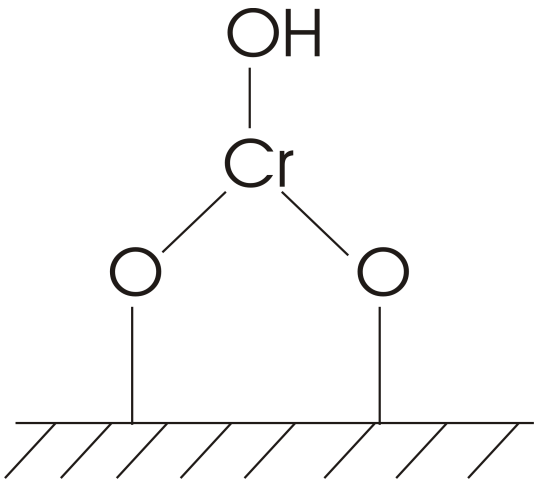

Figure 1.1: The Cr(III)G structure proposed in Ref. [17] to be active in catalytic dehydrogenation.

and reaction mechanisms to which they are applied. Furthermore, for simplicity of computation, ethane has been used as reactant in the modelling of catalytic dehydrogenation.

The surface of a Cr/oxide catalyst is too large and complex to be studied as a whole by quantum chemical methods. However, the active site on a Cr/oxide surface, at which the dehydrogenation reaction is catalyzed, is likely to be localized to only few surface atoms. In particular, the chemisorption of alkane has been proposed to involve a single chromium center or a chromium–oxygen pair [3, 17, 25, 47, 54]. Therefore, when modelling such a reaction by quantum chemical methods, the surface may be represented by the local site including the active atoms and their relative geometry. This constitutes the molecular-cluster-model approach, which has become popular due to three main advantages: (i) Moderate computational demands, which allows for (ii) the use of highly accurate methods, which (iii) are based on molecular orbital theory and thus provide a direct link between molecular chemistry and surface chemistry [60]. However, implicit in the molecular-cluster-model approach is neglect of the long-range electrostatic field and the structural constraints of the encapsulating surface [61]. Incorporation of these by an embedded-cluster approach may improve the description of the surface site [61, 62]. The 'naked' cluster does, however, serve as a tractable first approach, with merit in the description of local phenomena, both on alumina [63–65] and on silica [66].

The cluster-model approach allows the construction and study of a large variety of Cr/oxide surface species. For instance, a set of cluster models may be used to investigate the structure-reactivity dependency of catalytic dehydrogenation. Since chemical reactions are usually very fast, and the life-times of reaction intermediates are short, elucidation of the reaction path is difficult by way of experiment. Instead, using quantum chemical methods in conjunction with cluster models, the structures of reaction intermediates, transition states, and their relative energies, may be obtained with relative ease [67]. Different mechanisms for the catalytic dehydrogenation of ethane on a modelled Cr/oxide surface site may thus be composed and assessed based on the minimum

energy required for reactants to convert to products. It is thereby possible to perform a screening of many chromium surface species and reaction mechanisms.

A model-based study as outlined here, bears its strength in the implicit detail, which cannot be matched by experiment. However, to have any bearing on the understanding of the real system, it is essential to provide parameters that may be tested by experimental observation.

1.4 Aim, Approach, and Structure of the Thesis

The general aim of this thesis is to provide a new foundation for extended understanding of the Cr/oxide catalysts for dehydrogenation of short alkanes. In particular, the aim has been to identify the chromium surface structures that contribute most efficiently, the mechanism that is involved, and the role of the oxide support.

The approach has been; through review of the literature to develop a range of realistic candidate models of chromium surface species, to test these models through selected computations; and thereby provide new basis for interpretation of previously reported experimental observations, and, moreover, inspire novel experiments. Specifically, the computations pertain to mechanisms of catalytic dehydrogenation and reactions of catalyst precursors leading to the active catalyst.

The main computational methods used in this work are presented in Chapter 2, and the Cr/oxide surface models to which they are applied are presented in Chapter 3. Catalytic dehydrogenation is the topic of Chapter 4, which summarizes the results presented in Papers I-III. For this study, the family of chromium surface species was modelled to span a range of structural properties, and investigated with respect to mechanisms of catalytic dehydrogenation. In Chapter 5, an overview is given of the computational results presented in Paper IV. In this study, based on an experiment reported by DeRossi *et al.* [17], the reaction of Cr(II)/silica with water has been investigated. The reaction is of interest since DeRossi *et al.* [17] found the product Cr(III) species active in catalytic dehydrogenation, and furthermore proposed it as a candidate for the much discussed redox Cr(III) species. Concluding remarks and suggestions for further work follow in Chapters 6 and 7, respectively. Finally, the scientific papers I-IV are attached in numeric order.

Chapter 2

Computational Methods

Reactions of gas-phase molecules at surface sites of Cr/oxide involve the breaking and formation of chemical bonds. Furthermore, rearrangements of the oxide surface may take place beyond the local site. In the present computational approach to describe these processes, methods based on Quantum Mechanics (QM) and Molecular Mechanics (MM) have been applied, and models of reactive surfaces have been generated using Molecular Dynamics (MD).

In the following, a brief description is given of the main computational methods used. The methods are employed as implemented in generally available software, which in two cases have been adapted especially for the present purpose. For textbooks on the subject, confer Refs. [68, 69].

2.1 The Schrödinger Equation

The activation of chemical bonds is a quantum mechanical process. A description of the energetics and the structures involved may be obtained by solving the non-relativistic time-independent Schrödinger equation:

$$\mathcal{H}\Psi = E\Psi$$

The Hamiltonian operator, $\mathcal{H}$, of this eigenvalue problem determines the system in terms of spatial coordinates of the electrons and nuclei. The proper solution, Ψ, is the wavefunction for the system, and E is the energy.

Solving this eigenvalue problem is a complex task, which, for systems of more than one electron, requires an approach of several approximations. First, the movement of electrons and nuclei are assumed decoupled. This leads to the Born-Oppenheimer approximation of expressing the wavefunction as a product of electronic and a nuclear factors [70]. The assumption is a mild one, since electrons adjust almost instantly to changes in position of the much heavier nuclei. Thus, from the electron point of view, the nuclei may be considered as fixed in space. Manifested in the Schrödinger equation this gives an *electronic Hamiltonian*, which includes the static field of the nuclei, but not the nuclear kinetic term. The eigenvalues of this Hamiltonian are referred to as *electronic energies*,

and obtained as a function of the relative positions of the nuclei, define a Potential Energy Surface (PES). The relative motion of the nuclei is governed by this PES, equilibrium structures represent minima, and transition states are first order saddle points.

The nuclear wavefunction may be factored into translational, rotational, and vibrational parts, which are, respectively, solved within the ideal gas, rigid rotor, and harmonic oscillator approximations. The solutions can be used to obtain thermodynamic parameters.

The variational principle provides a starting point towards approximate solutions of the electronic wavefunction. This principle states that the expectation value of the Hamiltonian, using a trial wavefunction, is never lower in value than the true ground state energy of the true ground state wavefunction. This allows the construction of trial wavefunctions, which may be optimized systematically towards the proper solution of the system under study.

As a first approximation, non-interacting electrons may be assumed, and the many-electron wavefunction written as a product of single-electron wavefunctions. This is a Hartree product, and the single-electron wavefunctions are called molecular orbitals, each of which describes the motion of one electron without explicit dependency on the instantaneous motions of the other electrons in the system. However, in addition to the spatial coordinates, the electrons being fermions have an intrinsic spin coordinate designated as α or β. Furthermore, the antisymmetry principle states that the total wavefunction of a system of identical fermions is antisymmetric with respect to the interchange of any set of space-spin coordinates. For instance, interchanging the coordinates of two electrons changes the sign of the wavefunction. This is achieved by expanding the Hartree product as a Slater determinant [71]. This form of the wavefunction is also consistent with the result of quantum mechanics that electrons are indistinguishable. Finally, space and spin symmetry adapted wavefunctions are obtained as Configuration State Functions (CSF), which are linear combinations of Slater determinant terms with fixed parameters.

2.2 The Hartree-Fock Self-Consistent Field Approximation

In the Hartree-Fock (HF) or Self-Consistent Field (SCF) approach, the molecular orbitals of a single Slater-determinant wavefunction are obtained in a self-consistent iterative variational procedure in which the expectation value of the electronic Hamiltonian is minimized. The resulting wavefunction describes each electron as moving in the mean field of the other electrons. Hartree-Fock theory is therefore described as an independent particle model or a mean-field theory. In the formalism of Unrestricted Hartree Fock (UHF), all electrons are allowed different spatial orbitals, while the Restricted Hartree-Fock (RHF) equations are obtained under the additional constraint that pairs of electrons with opposite spin have the same spatial orbital [72, 73]. UHF is typically applied in the study of open-shell systems with unpaired electrons, while RHF is used for closed-shell systems with paired electrons. In the calculation scheme, each molecular orbital is expressed as an expansion of basis functions, usually atom-centered orbitals, and the coefficients are

determined under the variational constraint of orthogonal molecular orbitals [74, 75]. In practice, the choice of basis set introduces further approximations in the compromize between accuracy and computational requirements. Basis sets must be chosen large enough to give meaningful results, while small enough to make computations feasible.

2.3 Electron Correlation

The Hartree-Fock (HF) approximation does not account for the adjustment of electron motion to the instantaneous positions of all the electrons in the system. As described by the HF wavefunction, electrons of opposite spin may even occupy the same space at any instant. Though this is prevented for electrons of parallel spin, through exchange interaction ensured by the anti-symmetry form of the wavefunction, the electron-electron repulsion is overestimated. Therefore, when approaching the limit of an infinite expansion of basis functions, there is a lower bound on the HF energy which exceeds the exact non-relativistic electronic energy of the system. True to its origin, the gap between this HF limit and the exact energy is called the correlation energy. Generally, this amounts only to about 1% of the total electronic energy, but is on the same order of magnitude as the activation energy of chemical reactions [69]. Actually, the correlation energy is not only due to electrons avoiding each other, which is called the *dynamical* correlation energy. There is also a contribution called the *non-dynamical* correlation energy, which stems from the inadequacy of a single Slater-determinant wavefunction in describing certain electronic states. This is typically the result of near-degenerate states and rearrangement of electrons in partially filled shells. Cases where non-dynamical correlation energy may be important are; the dissociation of bonds, excited states, and the unpaired electrons in complexes of transition metals.

2.4 The Multi-Configurational Self-Consistent-Field Approximation

The non-dynamical correlation energy may be addressed by a multi-configurational Hartree-Fock method in which the wavefunction, expressed as a linear combination of Slater determinants, is optimized variationally with respect to simultaneous variations of the orbitals and the CSF coefficients. One implementation of such a Multi-Configurational Self-Consistent Field (MCSCF) method is the Complete Active Space Self-Consistent Field (CASSCF) approach [76]. By this method, the wavefunction is constructed by dividing the occupied orbital space into a set of inactive or closed-shell orbitals, and a set of active orbitals. Subject to symmetry restrictions, the electrons to be correlated are distributed in all possible ways in the set of *active* orbitals.

2.5 Many-Body Perturbation Theory

MCSCF or CASSCF calculations usually account only for a small percentage of the dynamical correlation energy. Therefore, to obtain accurate results, subsequent correlation treatments are usually applied. One approach is multi-reference perturbation theory. This is an example of many-body perturbation theory in which electron correlation is considered a perturbation to a zeroth order wavefunction of, e. g., non-correlating electrons. A second order perturbation estimate of the correlation energy of single reference wavefunctions is usually obtained by the Møller-Plesset (MP2) [77] approach. Multi-reference perturbation theory has been defined in several ways. The most popular extend to second order, such as the CASPT2 method of Roos *et al.* [78], and the MCQDPT2 method of Nakano [79]. These methods are not variational since the obtained energy does not represent an upper bound to the exact energy. However, this is generally not an issue when energy differences are considered. Moreover, these methods ensure correct scaling of the energy with the size of the system under study, which in many cases is more important than obedience to the variational prinicple.

2.6 Density Functional Theory

Density functional theory allows inclusion of correlation effects without applying costly wave-function methods. The energy is not obtained as eigenvalues of a wave function, but rather as a functional of the electron density. The method is based on two theorems by Hohenberg and Kohn [80], the first of which establish that the electron density of a system determines all ground state properties, and the second provides a variational principle. This was later exploited by Kohn and Sham [81] who introduced a formalism to minimize the energy as expressed by a density functional. Their trick was to introduce a fictitious system of non-interacting electrons with the same density as the interacting electrons of the real system. The first Hohenberg theorem assures that the positions of nuclei in the two systems are the same. The energy density functional was accordingly divided into kinetic energy and repulsion terms corresponding to non-interacting electrons and a correction term accounting for the interactive nature of the electrons. This correction term is known as the exchange-correlation density functional. The electron density was then expressed as the square of a single Slater-determinant wavefunction, and the Kohn-Sham equations derived under the variational constraint of orthonormal molecular orbitals. The equations are solved self consistently.

The beauty of the Kohn-Sham formalism is at least twofold. At computational cost similar to that of a simple HF calculation, the electronic properties could be resolved exactly, given the exact form of the exchange-correlation density functional. The potential savings in CPU time, has motivated considerable efforts towards approximating this functional. Most elementary is the Local Density Approximation (LDA) [82–85], which at each point in space, r, of local density, $n(r)$, applies the solution evaluated for a uniform electron gas with the same global density $n_o(r)$. For such computations, Slater provided a local-exchange functional [86] and Vosko, Wilk, and Nusairs provided a correlation functional [85]. LDA serves as starting point for a variety of gradient-corrected

functionals in which added terms account for the gradient of the electron density. A popular correction to Slaters local-exchange functional [86] was presented in 1988 by Becke (B) [87]. It may be applied in combination with a range of available gradient corrections to the local correlation functional. One popular choice was proposed by Perdew in 1986 (P86) [88]. The combined BP86 functional is an example of a 'pure' density functional. It differs from 'hybrid' density-functional approaches, in which the exchange functional is fitted empirically with a mixture of exact Hartree-Fock exchange. B3LYP is an example of a popular hybrid density functional with three parameters determined by fit to experimental data [89].

According to a recent review by Friesner *et al.* [90], density functional theory is at present the best approach for investigation of reactive chemistry in medium to large systems. Furthermore, it has proven successful in studies of transition-metal chemistry [91]. However, a drawback of density functional theory compared to wavefunction methods, is that it provides no method of systematic improvement towards the exact solution.

2.7 Molecular Mechanics and Molecular Dynamics

Determination of electronic structure by quantum mechanical methods is computationally expensive. In cases where only molecular structures and properties are needed, the computational model of Molecular Mechanics (MM) may be more practical. Based on the Born-Oppenheimer approximation as described in Section 2.1, the nuclear motions in a molecular structure, such as vibrations and rotations, can be studied separately from electrons. In molecular mechanics, focus is on the nuclear motion. Electrons and nuclei are put together in spherical atom-like particles, and the potential energy surface governing the relative movement of these is treated in terms of force fields. The force fields are parameters of atomic properties and bonding determined from experiment and from quantum mechanical computations on model systems. Atom types are defined with radii and net electronic charge, and by the form of bonds the atoms make with atoms of the same and other types. Bonds are considered as springs, which allow simple mathematical description of stretching, bending, and twisting deformations. Non-bonded atoms interact through van der Waals attraction, steric repulsion, and electrostatic interactions. The force field description accumulates in a total energy expression:

$$\mathrm{E}_{Total} = \mathrm{E}_{Stretching} + \mathrm{E}_{Bending} + \mathrm{E}_{Torsion} + \mathrm{E}_{Non-bonded\ interaction}$$

Molecular Dynamics By combining the force field of molecular mechanics and the Newtonian equations of motion, the displacement of atoms in a molecular structure can be computed over a time interval at defined temperature and pressure. This constitutes Molecular Dynamics (MD). The calculations of motion are done at discrete and small time intervals and a velocity is calculated on each atom position which in turn is used to calculate the acceleration for the next step.

The molecular mechanics and molecular dynamics computations in this thesis are performed with the General Utility Lattice Program (GULP) [92–94]. Molecular dynamics have been used in a method of simulated annealing to obtain realistic surface models of Cr/silica, cf. Chapter 3 and Paper I. Molecular mechanism have also been used in mechanical embedding (*vide infra*).

2.8 Mechanical Embedding

The treatment of extended surfaces entirely by quantum chemical methods can be computationally extremely expensive. In some cases, a more tractable approach is to model only a small region at the quantum chemical level, and the remainder of the extended system more approximately at the molecular mechanical level. This constitutes the method of Mechanical Embedding, or QM/MM [61,62]. There are several implementations of the general idea. They differ in the coupling of the quantum chemical and molecular mechanical regions. In one approach, frozen localized orbitals derived from model molecules are used at the interface between a QM and MM atom [95, 96]. More common is the use of "link atoms" to saturate the dangling bond at the frontier atom of the QM region [61]. For instance, in the case of silica, hydrogen atoms may be used to terminate dangling SiO– bonds. Furthermore, the treatment of the link atom in the computations offers many possibilities, and the energy expressions may be set up in different ways [61].

For the work in this thesis, QM/MM geometry optimizations were performed using the QM-Pot mechanical embedding program of Sierka and Sauer [97]. In this implementation, the total energy to be minimized is given by

$$E_{Total} = E_{host,MM} - E_{cluster,MM} + E_{cluster,QM}$$

The link atoms, i.e. the hydrogen atoms used to terminate the dangling covalent bonds of the cluster, were placed along the direction of the $O_{cluster}$–Si_{host} bond as $O_{cluster}$-H-Si_{host}, at a fixed distance from $O_{cluster}$. This is enforced during the QM/MM geometry optimization. As a result, the gradients on the $O_{cluster}$–Si_{host} bonds are due only to the host MM gradients [97]. For application in this thesis, the QM-Pot program was adapted to take input of QM energy and gradients from the Amsterdam Density Functional (ADF) set of programs [98].

2.9 Localization of Spin-Crossover Transition States

In typical chemical reactions the spin state is conserved throughout. In the language of quantum chemistry, the reaction proceeds on a single spin potential energy surface. However, in some cases there is a change of spin state in the course of the reaction. For instance, spin flip of the *d* electrons of chromium may take place during C–H activation upon formation of new Cr–C and Cr–H bonds. Owing to spin-orbit coupling, such reactions may proceed on a single adiabatic potential energy surface corresponding to the full electronic Hamiltonian. Such a reaction scheme, involving spin flip in the course of the

reaction is known as "two-state reactivity" (TSR) [99]. The role of TSR in C–H activation and other transition metal-catalyzed reactions, has recently been reviewed [100].

A critical point on the reaction coordinate of such a reaction is the Minimum Energy Crossing Point (MECP) between the spin-potential surface of the reactant and the product. Harvey et al. [101, 102] have implemented a method to locate such crossing points based on input from quantum chemical programs at each point in the geometry optimization. Energies and gradients for the two spin states are combined to produce an effective gradient pointing toward the MECP and used to update the geometry. In the course of the present work, the Unix scripts and Fortran programs of Harveys method were adapted to use with the Amsterdam Density Functional (ADF) set of programs [98].

2.10 A Brief Consideration of Accuracy

Density functional theory has been the main workhorse of this thesis, pulling as plough the BP86 functional [87, 88]. This level of computations has allowed the study of a range of reactions on many, and relatively large models of Cr/oxide surface species. However, it is important to be aware of the limitations of the method.

As computed by gradient corrected density functional theory, relative energies on a single potential surface are generally in agreement with more sophisticated methods [91, 103–106]. Relevant to the present study, differences of less than 15 kJ/mol have been obtained between hybrid DFT and higher-level theory for the insertion reaction of ethene into Cr(III)–alkyl bonds [103], and the BP86 'pure' density functional was found in agreement with more sophisticated methods concerning the same reaction on a titanium metal center [104]. Predicting relative energies on different potential surfaces is more problematic [107, 108]. A general trend of errors cannot be referred, though Poli and Harvey [108] report that 'pure' density functionals such as BP86 tend to exaggerate the stability of low-spin forms, whereas hybrid functionals such as B3LYP may overestimate the stability of high-spin species. Generally for the computations presented in this thesis, relative energy differences lower than 20 kJ/mol are considered to be within the error bars of the method.

Chapter 3

Models of Cr/oxide Surface Species

A major challenge in computational studies of any of the Cr/oxide systems is to develop realistic models of the chromium surface sites. The first step is to incorporate what is known and suggested based on experimental observations.

As outlined in the introduction to this thesis, chromium becomes anchored to alumina or silica supports in reactions with surface hydroxyl groups [18, 27, 39–43]. The local structure of the anchored chromium species thus depends on the nature of the hydroxyl groups. On surfaces of hydrated silica, the hydroxyl groups are of the type $HO(\text{-}Si)_1$, i. e. with oxygen coordinating to one silicon atom [60]. On hydrated alumina, there are two types of hydroxyl groups, $HO(\text{-}Al)_1$ and $HO(\text{-}Al)_2$, with oxygen coordinating to one or two aluminum atoms, respectively, see Ref. [109] and the references therein. Anchoring of chromium by reaction with these surface groups would give $Cr–O(–M)_1$ and $Cr–O(–M)_2$ links with doubly- and triply-coordinated oxygen, respectively. These structural properties are represented in the set of Cr/oxide models.

The dominant view in the modern literature is that +III is the most catalytically active oxidation state for dehydrogenation, possibly with minor contributions from +II [17, 18, 21, 26, 52, 53]. The set of surface models is therefore focused on Cr(III) for the purpose of modelling catalytic dehydrogenation, while models of Cr(II)/silica have been constructed for investigation of the oxidation of Cr(II) to Cr(III) on the surface of amorphous silica.

Cluster models have been constructed both in an *ad hoc* manner by identifying likely anchoring sites of chromium on low-index surfaces of silicalite and alumina, and systematically by simulated annealing of chromium on low-index surfaces of high-temperature silica crystals.

3.1 Models of Cr(III)/oxide

DeRossi *et al.* [17] have suggested that the active chromium center may be bonded to the surface *v*ia two Cr–O–M bridges and with hydroxyl as the third ligand, cf. Fig. 1.1 in Chapter 1 of this thesis summary. From its spectroscopic signature, the species was named Cr(III)G. We have taken this structure as our starting point, and explored the more general, conceptual model of *Cr(III) complexes with three covalent ligands coordinating through oxygen.*

The cluster models of Cr(III)/oxide that have been studied in Papers I, II, and III, are presented in Fig. 3.1. An additional model that represents a special case of the Cr(III)G species is presented in Fig. 3.2. The computational results obtained with this latter model has been included in this thesis summary, but are not reported elsewhere.

The structure of all the models have been optimized to minima on the respective potential energy surfaces, the *ad hoc* cluster models at the quantum mechanical (QM) level, and the systematic models at the QM/MM level. The structural parameters describing the active chromium center in each model are included in Tab. 3.1.2.

3.1.1 *Ad hoc* Cluster Models

Brief descriptions of the *ad hoc* cluster models are given here. More detailed descriptions are presented in Papers I and III.

The essence of a Cr(III)G species as proposed by DeRossi *et al.* [17] is maintained in model **A** in Fig. 3.1. The model represents a hydroxychromium(III) species anchored by two doubly coordinated oxygen links on the (100) face of γ-alumina. O–Al links to the extended surface are considered as cut, and the open valencies filled using hydrogen atoms. See Paper III for more details.

A variation of the Cr(III)G structure is three-bridge chromium, which would result from a condensation reaction involving the hydroxyl ligand of two-bridge chromium and a vicinal hydroxyl group on the surface. The 3bridge-alumina model shown as Fig. 3.1**G** represents such a chromium(III) species. Here, chromium is anchored *via* triply coordinated oxygen to the (001) face of α-alumina. For more detail see Paper III.

A general model of two-bridge Cr/silica has been constructed with the silica surface represented by a di-siloxyether molecule, cf. Fig. 3.1**B**. The hydoxychromium center is anchored *via* doubly coordinated oxygens. In the model, SiO–Si bonds to the extended surface are considered as cut and the dangling bonds terminated by hydrogen atoms. This cluster model is central in the study of mononuclear Cr(III)/silica presented in Papers I and II.

Turning to species of polynuclear chromium, a Cr(III)G-type center may be linked to the surface *v*ia Cr–O–Cr links, i. e. one or more chromium atoms may take the place of neighboring silicon or aluminum atoms of the oxide surface. The diCr-silica model in Fig. 3.1**C**, represents such a site of dinuclear chromium on a silica surface. Two hydroxychromium(III) centers are connected by a Cr–O–Cr link, and each chromium center is anchored to a surface silicon *via* doubly coordinated oxygen. The silica surface is modelled by a di-siloxyether molecule, same as in model **B**, though a different orientation was obtained when optimizing the structure to a minimum on the potential energy surface.

The 2bridge-chromia model in Fig. 3.1**D** is constructed to be a simple model of Cr(III)G-type centers situated on amorphous chromia. The model is composed of three hydroxychromium(III) centers linked by Cr–O–Cr bridges with twofold coordinated oxygens, and the geometry relaxed to a minimum on the potential energy surface. One or more of the hydroxyl groups may be viewed as a severed Cr–O–M link, M=Al, Si, Cr

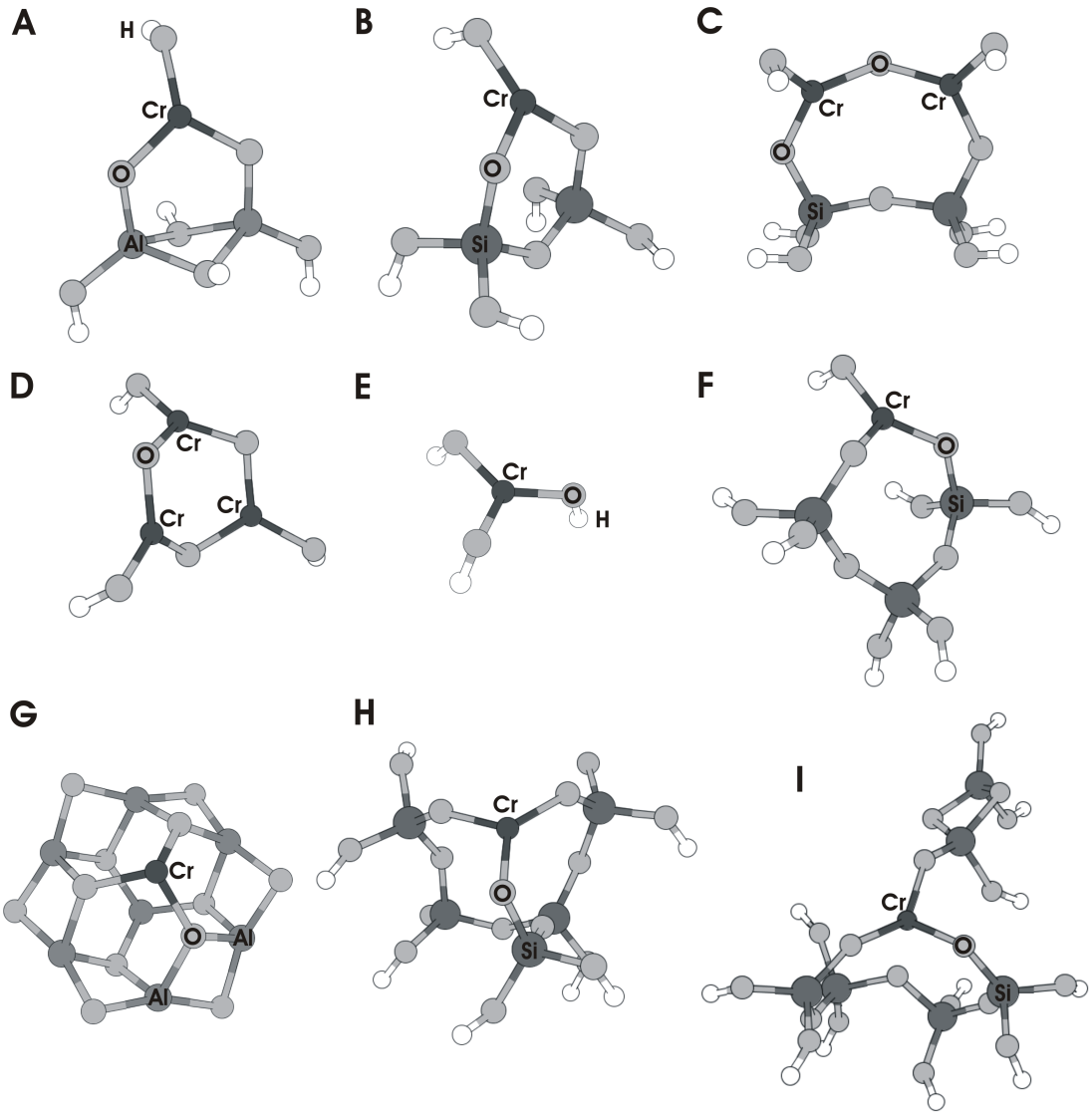

Figure 3.1: Cluster models representing variations of the Cr(III)G-type species proposed by DeRossi to be active in catalytic dehydrogenation; 2bridge-alumina (**A**), 2bridge-silica (**B**), diCr-silica (**C**), 2bridge-chromia (**D**), $Cr(OH)_3$ (**E**), 2bridge-silica (**F**), 3bridge-alumina (**G**), 3bridge-silica (**H**), and 3bridge-silica (**I**).

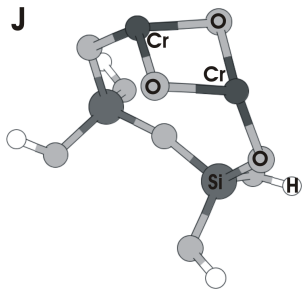

Figure 3.2: Cluster model **J** represents a realization of the dinuclear Cr(-O-)$_2$Cr/silica species proposed by Groeneveld *et al.* [34, 110] and Wittgen *et al.* [111, 112].

depending on the support, where the dangling bond has been terminated with hydrogen.

The first coordination sphere of chromium in the Cr(III)G species is even reproduced by the Cr(OH)$_3$ molecule, see Fig. 3.1**E**, which defines a site completely void of surface constraints.

In addition to the covalently bonded oxygen ligands, other surface oxygen species may act as Lewis donors coordinating to the chromium center. Examples on silica are adsorbed water, silanols and siloxanes. For simplicity the effect on reactivity has been studied in Paper I by means of a water molecule pre-coordinated to chromium in the two-bridge Cr/silica model **B** and the Cr(OH)$_3$ model **E** in Fig. 3.1.

A Special Case of the Cr(III)G species Sites of polynuclear chromium probably offer a variety of surface structures. For instance, two chromium(III) centers, both with three ligands coordinating through oxygen, may be linked by two Cr–O–Cr bridges instead of one, thus forming a four-membered Cr(-O-)$_2$Cr ring structure. This structure was actually proposed by Groeneveld *et al.* [34, 110] and Wittgen *et al.* [111, 112] to be the oxidation product of a dinuclear chromium(II) species and water or silanols on a silica surface. Model **J** in Fig. 3.2 is a realization of their proposal. Cr–O–Si links anchor each chromium atom to the silica surface, which is modelled by a di-siloxyether molecule.

3.1.2 Systematic Models of Cr(III)/silica

For the study of mononuclear Cr/silica in Paper I, improved models taking into account larger parts of an amorphous silica support were generated from low-index surfaces of the high-temperature modifications of silica; α- and β-cristobalite. Molecular dynamics in conjunction with shell-model potentials was used to obtain structurally relaxed slab models of Cr/silica surfaces, cf. Fig. 3.3. The details of the procedure as applied in this work are described under Computational Details in Paper I. For a broader introduction see e.g. Ref. [113].

As illustrated in Fig. 3.3, a cluster region was defined subsequent to the annealing process. This region includes chromium and its local chemical environment, with boundary $O_{cluster}$–Si_{host} bonds severed and terminated by hydrogen atoms. These clusters were

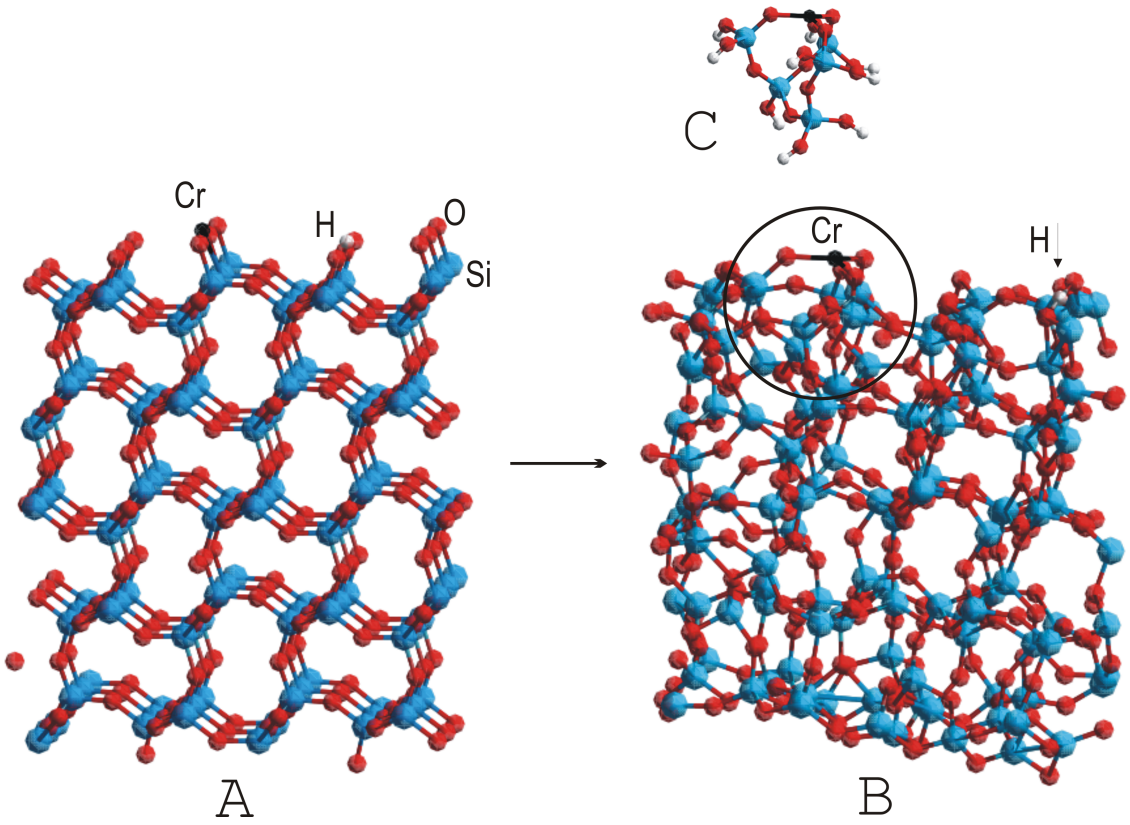

Figure 3.3: Systematic preparation of Cr/silica surface models using simulated annealing. A: The unrelaxed surface with Cr, H and O added; B: The fully relaxed slab model following simulated annealing and optimization; C: Cluster model with hydrogen-terminated dangling bonds. (The figure is adapted from Plate 1 in Paper I).

Table 3.1: The local geometry about chromium in the clusters.

Cluster[a]	∠OCrO[b]	rCrO[b]
A 2bridge-alumina	123.8, 123.7, 110.3	1.80, 1.80, 1.80
B 2bridge-silica	123.9, 123.9, 107.7	1.81, 1.81, 1.78
C diCr-silica	117.9, 119.9, 121.6	1.82, 1.79, 1.79
D 2bridge-chromia	122.0, 121.9, 114.4	1.79, 1.79, 1.80
E $Cr(OH)_3$	120.0, 120.0, 120.0	1.79, 1.79, 1.79
F 2bridge-silica	120.2, 119.7, 119.4	1.80, 1.80, 1.79
G 3bridge-alumina	102.8, 102.8, 103.1	1.80, 1.80, 1.80
H 3bridge-silica	130.3, 118.0, 110.4	1.83, 1.82, 1.77
I 3bridge-silica	139.2, 113.1, 105.5	1.93, 1.92, 1.84
J $Cr(\text{-}O\text{-})_2Cr$-silica	121.0, 87.2, 121.0	1.82, 1.82, 1.82
K Cr(II)-silica	112.1	1.82, 1.82
L (Cr(II)OH)-silica	129.7	1.88, 1.82
M $(Cr(II)OH)_2$-silica	146.6	1.85, 1.78

[a] Cluster labels are defined in Figures 3.1, 3.2, and 3.4.
[b] Units: Bond lengths (r) in Å, angle (∠) in degrees.

used separate from the bulk in pure quantum mechanical (QM) cluster calculations, and as the QM region in QM/MM periodic boundary calculations. For details see Paper I.

From the (100) face of α-cristobalite, a two-bridge Cr(III)OH species was generated. The cluster model is presented in Fig. 3.1**F**. Three-bridge Cr(III) models were generated from the (101) and (111) faces of β-cristobalite, confer models **H** and **I** in Fig. 3.1. Forces exerted by the extended surface cause distortion of the local geometry around chromium in the three-bridge model **I**, cf. Table 3.1.2. On the other hand, the two- and three-bridge Cr/silica models, **F** and **H**, respectively, are geometrically quite relaxed.

3.2 Cluster Models of Cr(II)/silica

Models of Cr(II)/silica have been constructed for the investigation of different parts of the reaction between Cr(II)/silica and water.

By experiment, it has been found that exposing calcined Cr/silica catalyst to CO, Cr(VI) species are reduced to Cr(II) [16, 17, 32, 34, 114]. The oxo ligands are removed in the process, [42,49] and the product chromium(II) center has been depicted as bonded to silica *via* two Cr–O–Si links [115,116]. For Cr/silica with a chromium load below 2 wt%, the Cr(VI) species on the calcined surfaces are found to be mononuclear [116, 117], and the nuclearity is conserved during reduction by CO of Cr(VI) to Cr(II) [32].

Model **K** in Fig. 3.4 represents mononuclear chromium(II) bound to silica *v*ia two Cr–O–Si links. It has been used to study hydrolysis of Cr–OSi links. The silica surface is modelled by a di-siloxyether molecule, which after relaxation of the cluster geometry takes the same orientation as in model **B** of a two-bridge Cr(III) species.

Model **L** in Fig. 3.4 represents a Cr(II)OH moiety anchored to an amorphous silica

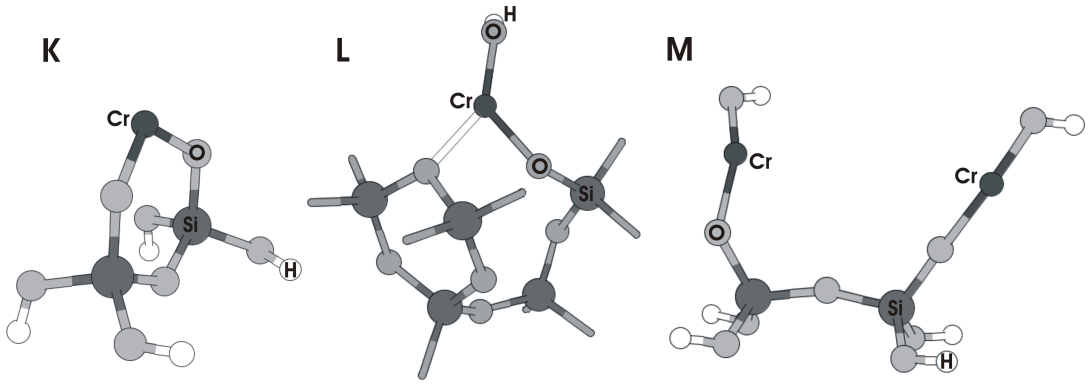

Figure 3.4: Cluster models of Cr(II) on silica: mononuclear Cr(II)/silica (**K**), mononuclear Cr(II)OH/silica (**L**) and two mononuclear Cr(II)OH moieties anchored on vicinal silicon atoms of a silica surface site (**M**). Polar-covalent bonds are represented by colored sticks, while dative bonds are represented by blank sticks. (Figure 1 of Paper III).

surface by a single Cr–O–Si linkage, and with chromium bonded datively to a surface siloxane. The model was made with the purpose to study the ability of a Cr(II)OH moiety to travel across a silica surface. It was constructed by adaption of model **H** in Fig. 3.1.

Finally, model **M** in Fig. 3.4 has been constructed for the purpose of studying the reaction between two Cr(II)OH moieties on the surface of amorphous silica. Also for this model the di-siloxyether molecule is used to model the silica surface. Details of preparation are given in Paper IV.

Chapter 4

Catalytic Dehydrogenation

With aim to elucidate the relation between structure and catalytic activity, the Cr(III)/oxide models presented in Chapter 3 have been studied computationally with respect to catalytic mechanisms of ethane dehydrogenation. The results are presented in Papers I, II, and III, and are summarized in Section 4.4 below. In the following, an overview is given with basis in the scientific papers, starting with a brief review of the literature with respect to mechanistic information.

4.1 Mechanistic Information from the Literature

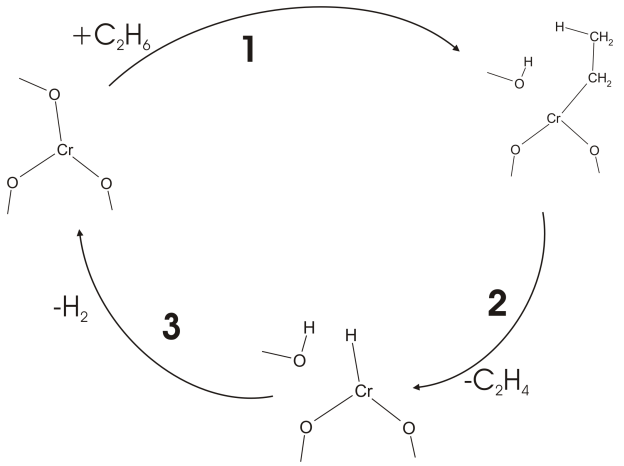

Figure 4.1: Schematic reaction mechanism for dehydrogenation of ethane over Cr/oxide as proposed by Weckhuysen and Schoonheydt [3]. (Figure 2 of Paper I.)

In the most recent review of Cr/oxide catalysts for dehydrogenation of short alkanes, Weckhuysen and Schoonheydt [3] proposed that dehydrogenation may be initiated by physisorption of alkane on coordinatively unsaturated Cr(III) centers. Three subsequent steps were discussed which are in reverse order of those in an earlier proposal regarding

catalytic hydrogenation of ethene [118]. According to their proposal, activation of a C–H bond involves the formation of new O–H and Cr–alkyl bonds, cf. reaction **1** in Fig. 4.1. The alkene is then formed as a result of β-hydrogen transfer from the alkyl to chromium in reaction **2**. Regeneration of the catalytic site under formation of H_2 concludes the catalytic cycle, cf. reaction **3** in the figure.

The involvement of a chromium-oxygen pair in the C–H activation step is a recurring idea in the literature [3, 17, 24, 47]. However, the available mechanistic information is scarce, we have therefore considered reaction mechanisms systematically, based on the different mechanisms of C–H activation that are known from homogeneous organometallic chemistry. The two most relevant ones are oxidative and electrophilic addition [119]. Electrophilic addition is also known as σ-bond metathesis (σBM) [120], since metal–ligand and C–H bonds are replaced by metal–carbon and ligand–hydrogen bonds. Such a reaction is presented schematically in the upper part of Fig. 4.2. Conversely, in Oxidative Addition (OA) of the alkane, carbon and hydrogen binds directly to the metal as the C–H bond is broken, confer the lower part of Fig. 4.2. This reaction involves formal oxidation of chromium and change of spin state. It is thus an example of 'Two-State Reactivity' (TSR) [99]. The role of TSR in C–H activation and other transition metal catalyzed reactions, has recently been reviewed by Harvey *et al.* [100].

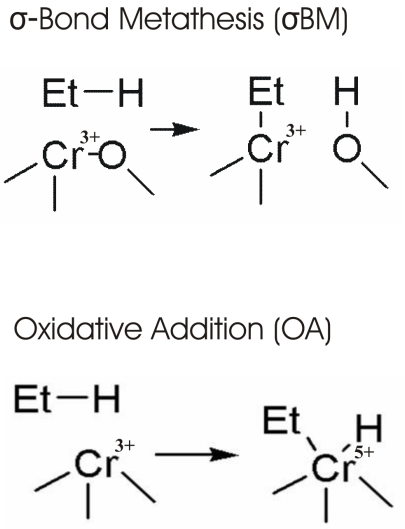

Figure 4.2: Schematic presentation of C–H bond activation in ethane (Et–H) at a chromium(III) center by σ-bond metathesis (top), and by oxidative addition (bottom).

In general, C–H activation by σ-bond metathesis is favored on light, electron-deficient metals, whereas oxidative addition is favored on the heavy and electron-rich late transition metals [2, 6, 91, 121]. There are, however, exceptions to this rule [120, 122, 123]. For instance, mechanisms of σ-bond metathesis have been proposed on platina complexes used in the Shilov-type system [120, 122], while $(DMPE)_2FeH_2$ is an example of a first-row transition metal complex capable of undergoing reactions that result in oxidative addition of alkane C–H bonds [123]. Although chromium is a first-row transition metal,

oxidative addition cannot be ruled out *a priori*. Oxidative addition has actually been found feasible on O=Cr=O and Cr=O molecules [124]. Furthermore, H_2 activation by oxidative addition has been reported for a Cr(III) complex with three ligands coordinating *via* nitrogen [125]. The complex is similar in essence to the Cr(III)G species proposed as active in dehydrogenation by DeRossi *et al.* [17], and illustrated in Fig. 1.1 in Chapter 1 of this thesis summary.

4.2 Modelled Catalytic Dehydrogenation of Ethane

Judging from the computations, a molecular complex does not form between ethane and chromium on the modelled sites of Cr(III)/oxide. This implies that the initial encounter is reactive rather than physisorptive, contrary to the proposal of Weckhuysen and Schoonheydt [3]. Based on the literature as briefly reviewed above, we have assumed the initial reactive collision between the chromium site and ethane to follow a mechanism of σ-bond metathesis or oxidative addition.

4.2.1 C–H Activation by σ-Bond Metathesis

In Paper I of this thesis, models of mononuclear Cr(III)/silica are investigated with respect to catalytic dehydrogenation of ethane based on C–H activation by σ-bond metathesis. The role of the oxide support and nuclearity of chromium is addressed in Paper III.

Four-centered transition states have been obtained for the C–H activation in ethane. This is in line with the description of the reaction as σ-bond metathesis. The C–H bond and a Cr–O bond of the surface species are broken simultaneously with the formation of new Cr–C and O–H bonds. By means of cluster models, we have investigated the reaction involving Cr–OM bonds, where M=H, Al, Si, and Cr, cf. Paper III. Furthermore, the effect of strain exerted on Cr–OSi bonds by an extended silica surface has been studied in Paper I by means of slab models and mechanical embedding, QM-MM, which is briefly described in Chapter 2. Dependencies on structural properties and of the oxide support being silica, alumina, or chromia, have thus be addressed. In general, the C–H activation energies range between 120 and 160 kJ/mol, while somewhat lower barriers are obtained in the cases where the Cr–O bond is weakened by structural strain (*v*ide infra).

Below, the results are presented by example of model **A** in Fig. 3.1, which represents a two-bridge CrOH species on an alumina support. In the initial reaction of this species with gas-phase ethane, a C–H bond may react in a metathesis reaction involving either the Cr–OH bond, or one of the Cr–OAl links, cf. Fig. 4.3. In either case, an ethyl ligand is formed on chromium; the difference lies in the formation of a water molecule, or a surface hydroxyl group, respectively. Considering the computed activation enthalpies of 146 and 138 kJ/mol, respectively, the two reactions appear equally feasible.

In the continuation of the C–H activation step, we have studied two different routes leading to catalytic dehydrogenation. One conforms to the proposal by Weckhuysen and Schoonheydt [3] which, apart from the absence of molecular adsorption of ethane, appears viable as the cycle of reactions **1**, **2**, and **3** in Fig. 4.1. The reaction is initiated

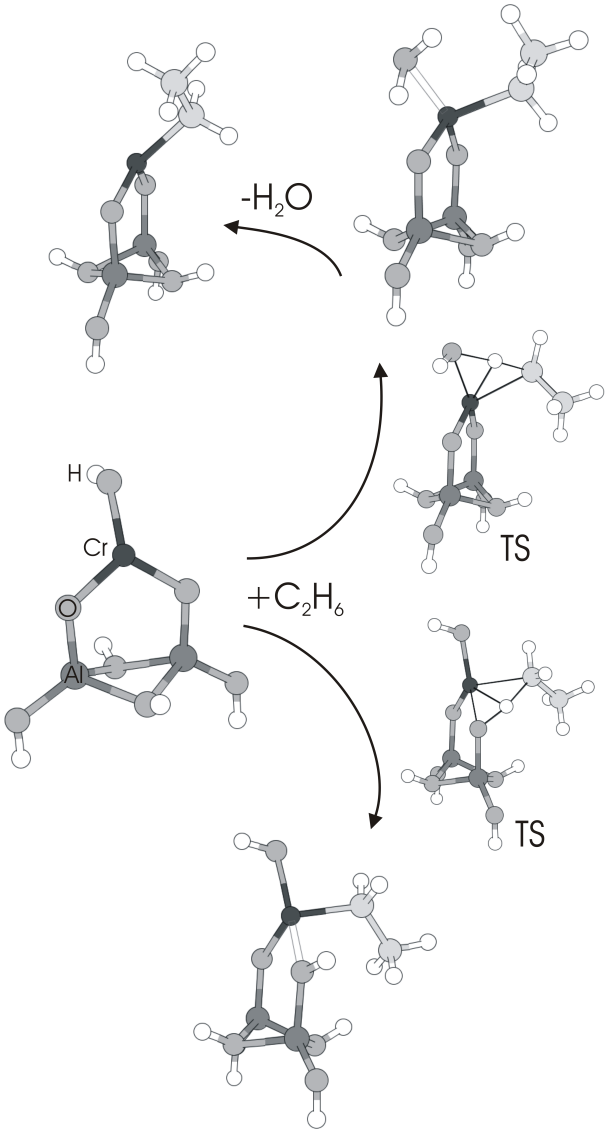

Figure 4.3: Optimized structures of stationary and transition states (TS) for the activation of a C–H bond in ethane by σ-bond metathesis involving cleavage of a Cr–OH (top) or a Cr–OAl bond (bottom) in the two-bridge Cr/alumina model catalyst **A**. Polar-covalent and dative bonds are represented by colored and blank sticks, respectively.

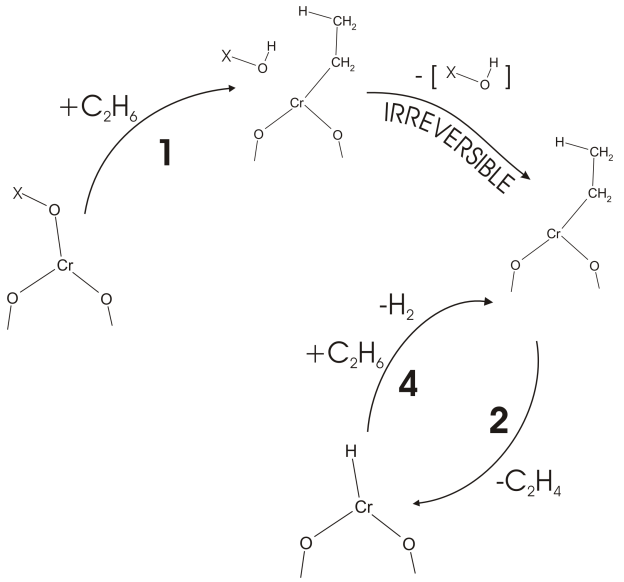

Figure 4.4: Schematic reaction mechanism for the irreversible C–O activation of a Cr(III) complex. In reaction **1** a Cr–OX bond is cleaved, here X represents a hydrogen, or a structural metal ion of the oxide surface. Irreversible loss of the XOH moiety from the chromium site opens for catalytic dehydrogenation according to the σBM/CrH cycle of reactions **4** and **2**.

and completed, respectively, by cleavage and reformation of a Cr–O bond through σ-bond metathesis, and will be referred to as the *σBM/CrO* mechanism.

With the exception of structurally strained surface species, the consistency between the various models is very good with respect to the energies computed for the reaction steps of the σBM/CrO mechanism (*v*ide infra). However, completion of the catalytic cycle by reformation of the Cr–O bond according to reaction **3** in Fig. 4.1 depends on a hydroxyl moiety or a water molecule remaining near chromium. Unless the surface site includes some spectator hydroxyl moiety, or steam is included in the feed, it becomes essential that the hydroxyl moiety or water molecule that is formed in the C–H activation step does not depart from chromium. However, judging from the computations, water binds only weakly to chromium, the coordination energies are obtained in the range of 30-80 kJ/mol for the models studied. Furthermore, at the typical reaction temperatures of dehydrogenation the increase in translational freedom as water desorbs gives a significant negative free energy change. For instance, C–H activation involving the Cr–OH bond of the two-bridge Cr/alumina model **A**, renders a water molecule which coordinates to chromium by 41 kJ/mol. At a reaction temperature of 500°C, the change in entropic upon desorption of water results in a change in free energy of -64 kJ/mol. This means that water is likely to desorb, as illustrated in Fig. 4.3. Thus, under dry reaction conditions reaction **1** becomes irreversible and the σBM/CrO cycle is terminated, cf. Fig. 4.4. Consistent catalytic activity according to the σBM/CrO mechanism is therefore likely to involve C–H activation at a Cr–O link to the surface, rather than a Cr–OH bond.

Despite the σBM/CrO mechanism being terminated by irreversible cleavage of the Cr–O bond, the surface site might still participate in catalytic dehydrogenation. In fact, an opening appears to be made for an alternative and energetically favourable mechanism. A hydridochromium complex is formed in reaction **2** of the σBM/CrO mechanism and if not consumed in reaction **3**, it may survive to accommodate the activation of a second alkane, which may involve the cleavage of a Cr–H bond and reformation of the ethyl ligand on chromium. This C–H activation reaction, schematically illustrated as step **4** in Fig. 4.4, is also one of σ-bond metathesis, and the sequence with reaction **2** constitutes a catalytic cycle which will be referred to as the *σBM/CrH* mechanism, cf. Fig. 4.4.

The main points described above were first reported in Paper I, which concerns the catalytic dehydrogenation of ethane over mononuclear Cr/silica. However, Cr/alumina is more interesting from an industry point of view. In the following, the σBM/CrO and σBM/CrH mechanisms of catalytic dehydrogenation are therefore presented by example of model **A** in Fig. 3.1 in Chapter 3, which represents a two-bridge Cr/alumina species. The results pertaining to the remaining Cr/oxide models in Fig. 3.1 are covered with less detail in an attempt to convey the relation between chromium speciation and catalytic activity. Some unpublished results are also included which concerns the catalytic dehydrogenation of ethane on the dinuclear chromium site represented by model **J** in Fig. 3.2.

Catalytic Dehydrogenation Involving a Cr–O Bond

The reaction coordinate along a cycle of the σBM/CrO mechanism traverses the sequence of three elementary reactions numbered in Fig. 4.1. Briefly described, C–H activation by σ-bond metathesis in reaction **1** gives an ethylchromium center and hydroxyl moiety in close interaction. Reaction **2** then proceeds by transfer to chromium of a β-hydrogen from the ethyl group. A hydridochromium complex is thus formed, from which ethene desorbs to the gas phase. Finally, in reaction **3**, the hydridochromium and hydroxyl moieties react by σ-bond metathesis to regenerate the catalytic site under release of H_2 to the gas phase. The optimized structures of transition states and reaction intermediates along this reaction coordinate on the two-bridge Cr/alumina species of model **A**, are presented in Fig. 4.5 together with a graphic representation of the changes in enthalpy and free energy. The catalytic σBM/CrO cycle is also illustrated in the lower part of Fig. 4.6. Note that the C–H activation step takes place at a Cr–OAl bond.

A detailed description of the σBM/CrO mechanism on model **A** is presented in the Results section of Paper III. However, since the mechanism and each of the elementary reaction steps are central to this thesis, they are described in some detail also here.

In reaction **1**, the enthalpy of C–H activation is 138 kJ/mol, and at 500°C, the change in entropy as ethane chemisorbs on the surface adds 118 kJ/mol to the Gibbs free energy of activation, which thus amounts to 256 kJ/mol. Simultaneously with the formation of a chromiumethyl complex, hydrogen is transferred to one of the oxygen bridges, which is converted into a surface hydroxyl. While polar-covalently bonded to aluminum, the hydroxyl moiety forms a weak dative bond to chromium. This is illustrated by a blank stick in Fig. 4.5. Relative to the reactant asymptote of the unreacted cluster model and

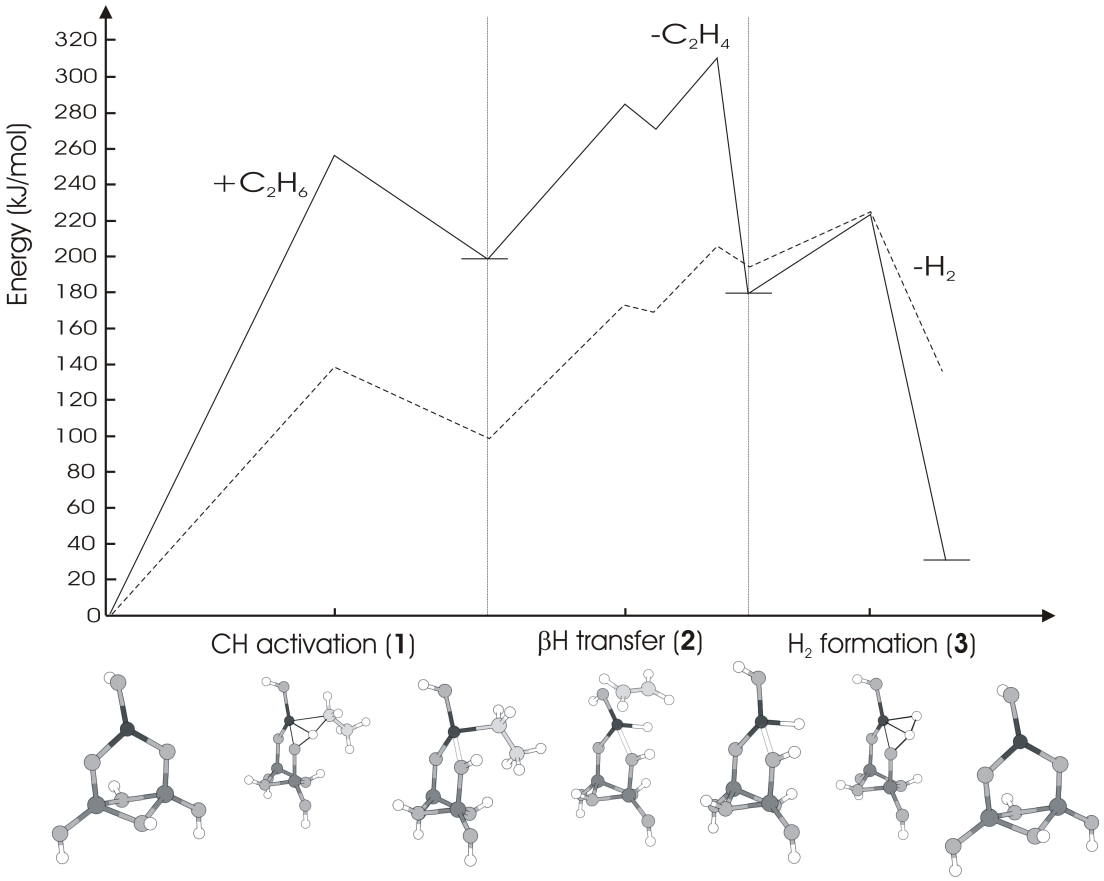

Figure 4.5: Optimized structures and plot of the changes in enthalpy (dashed line) and free energy (full line) along the reaction coordinate of the σBM/CrO mechanism as obtained for model **A** in Fig. 3.1. The thermodynamic functions are given in kJ/mol relative to that of the model catalyst and gaseous ethane. The reaction steps are (**1**) C–H activation of ethane by σ-bond metathesis involving a Cr–OAl bond, (**2**) β-H transfer to chromium with subsequent desorption of ethene, and (**3**) Cr–O formation with subsequent loss of H_2. Polar-covalent and dative bonds are represented by colored and blank sticks, respectively. (The figure is adapted from Fig. 5 of Paper III.)

gas-phase ethane, the enthalpy and free energy of this product are elevated by 99 and 198 kJ/mol, respectively.

Proceeding along the coordinate of reaction **2**, a β-hydrogen from the ethyl ligand transfers to chromium, and the energy increases almost all the way to the primary product, in which ethene remains weakly bound to the hydridochromium center, cf. Fig. 4.5. In terms of electronic energy, the transition state of β-hydrogen transfer lies 86 kJ/mol above that of the reactant ethylchromium complex, and only few kJ/mol above the product chromiumhydrido-ethene complex. Furthermore, at 500°C the enthalpy difference between transition state and product nearly vanishes. Immediate decoordination of ethene is therefore essential in order to prevent the hydrogen-transfer reaction from running backwards, and the reaction is driven forward by the increase in entropy as ethene desorbs to gain translational freedom. The entropic contribution to the free energy balances the increase in electronic energy relative to the ethylchromium complex such that the net change in free energy of step **2** becomes slightly negative. Confer the plot in Fig 4.5.

The exact position of the transition state of reaction **2** is difficult to ascertain since it is given by the maximum in free energy which most likely occurs somewhere along the path of ethene desorbing. The free energy increases with the electronic energy until ethene gains translational freedom, which most likely happens after the coordinative bond is broken. In this case, an enthalpy of activation may be estimated by adding the electronic coordination energy of ethene to the reaction enthalpy of β-hydrogen transfer. Relative to the ethylchromium complex, the activation enthalpy and activation free energy of reaction **2** thus becomes 108 and 111 kJ/mol, respectively.

Finally, with the hydroxyl moiety that is formed in reaction **1** remaining near chromium, the σBM/CrO mechanism may be completed according to reaction **3** as illustrated in Figures 4.5 and 4.6. The enthalpy and free energy of activating this final step are merely 28 and 43 kJ/mol, respectively. Reforging of the Cr–OAl bond is associated with an enthalpic change of -58 kJ/mol. Furthermore, release of H_2 to the gas phase contributes to a change in free energy of -148 kJ/mol.

Reaction Kinetics The relevance of the cycle of elementary reaction steps as a catalytic process is determined by the change in Gibbs free energy from the reactant asymptote of the separated cluster model and ethane, to the maximum along the reaction coordinate. This is the free energy of activation. It amounts to 309 kJ/mol for the σBM/CrO mechanism as computed for model **A**. Correspondingly, the bottleneck of the reaction path is the point on the reaction coordinate that corresponds to maximum free energy. The elementary reaction during which this point is reached is the rate-determining step. Conferring Fig. 4.5, this appears to be reaction **2**; the combined reaction of β-hydrogen transfer and desorption of ethene. Furthermore, the enthalpy of activation is obtained as the change in enthalpy going from reactants to the structure along the reaction coordinate that corresponds to the maximum in Gibbs free energy. For model **A**, the activation enthalpy of the σBM/CrO mechanism amounts to 207 kJ/mol.

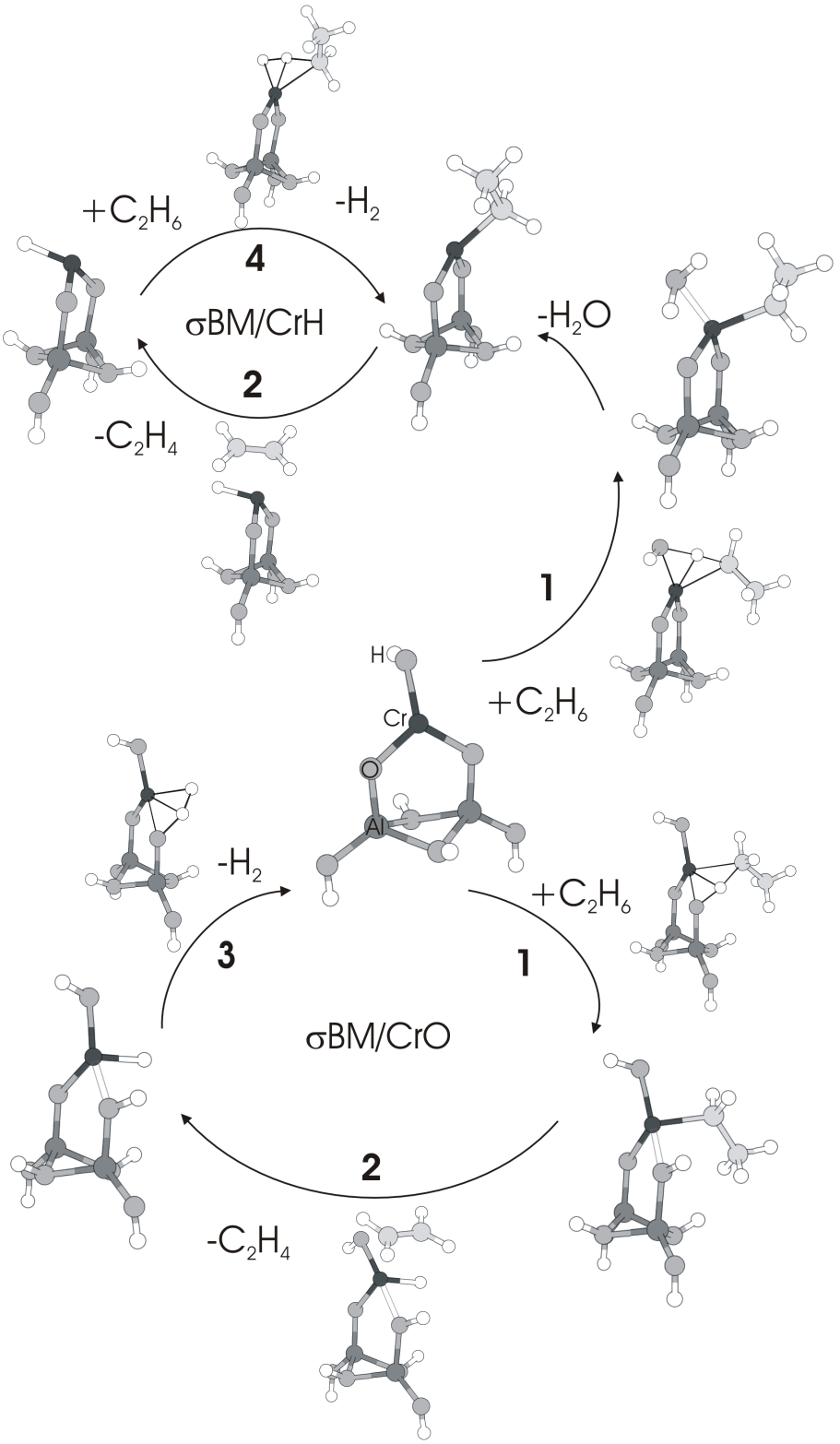

Figure 4.6: Optimized stationary structures for the σBM/CrO and σBM/CrH cycles of catalytic dehydrogenation of ethane over the two-bridge Cr/alumina model catalyst. The reaction steps are, (**1**) C–H activation of ethane by σ-bond metathesis at a Cr–O bond, (**2**) β-H transfer to chromium with subsequent loss of ethene, (**3**) Cr–O formation with subsequent loss of H_2, and (**4**) C–H activation of ethane by σ-bond metathesis at a Cr–H bond with subsequent loss of H_2. Polar-covalent and dative bonds are represented by colored and blank sticks, respectively. (The figure is a modification of Figure 3 of Paper III.)

The Structure-activity Relationship Identification of the rate-determining step based on thermodynamic functions, requires frequency analysis of the optimized stationary structures and transition states along the reaction coordinate. This has been performed for models **A** and **B** in Fig. 3.1 in Chapter 3, which represent species of two-bridge Cr/alumina and two-bridge Cr/silica, respectively. The results obtained for model **B** are reported in Paper I and the results obtained for model **A** are reported in Paper III. For these models, the profiles of electronic energy along the reaction coordinate closely resemble the profiles of enthalpy. Furthermore, the main entropic contribution to the free energy changes is the loss of translational freedom upon chemisorption of ethane, and the subsequent gain of translational freedom upon desorption of ethene and H_2 product molecules. This is model independent, and at 500°C amounts to 130 and 106 kJ/mol, for ethene and H_2, respectively. Taking into account changes in vibrational and rotational degrees of freedom and the pressure-volume work, the entropic contribution is modified to around 100 kJ/mol. These corrections are also fairly transferable between models. It thus appears that once the rate-determining step is identified, variations in activation energies with the structure of the chromium species may be investigated based on electronic energies.

Similar geometries of transition states and reaction intermediates to those presented in Figures 4.5 and 4.6, have been obtained for most of the Cr(III)/oxide models. The exceptions pertain to model **I** in Fig. 3.1 and model **J** in Fig. 3.2 which are characterized by structural strain. This will be discussed below. For the models of structurally quite relaxed chromium species, the gross features of the electronic energy profiles are quite consistent, cf. Fig. 4.7. Taking into account the negative entropy change as ethane chemisorbs and the positive change as ethene desorbs, reaction **2** appears to determine the reaction rate. Differences in the local surroundings of chromium, renders activation energies for the σBM/CrO mechanism in the range of 200 to 250 kJ/mol.

Activation energies of around 200 kJ/mol are obtained for the σBM/CrO mechanism involving C–H activation at a Cr–OM bond, M=Al, Cr, Si of two-bridge CrOH species on alumina, silica and chromia, respectively. Slightly higher activation energies around 250 kJ/mol are computed for the catalytic cycle involving cleavage of a Cr–OSi bond of the three-bridge Cr/silica model **H** in Fig. 3.1, or of a Cr–OAl_2 bond on three-bridge Cr/alumina model **G** in the same figure. The magnitude of the barrier reflects the energy of the hydridochromium complex with respect to the reactant asymptote of separated cluster and ethane. The silanol formed by C–H/Cr–OSi activation on model **H** coordinates poorly to chromium for structural reasons. The hydridochromium complex is thus destabilized relative to the reactant asymptote of separated cluster model and ethane, cf. Paper I. On the other hand, the hydridochromium complex formed by activation of a Cr–OAl_2 bond in model **G** appears to be destabilized due to polarization of the Cr–H bond, for more details see Paper III.

Significance of Surface Relaxation The results presented above for Cr/silica are based on cluster models in which the positions of the outer $Si(OH)_n$ groups were frozen. This constrained cluster-model approach exaggerates the structural rigidity in the silica support. Therefore, in Paper **1** mechanical embedding, QM-MM, as described

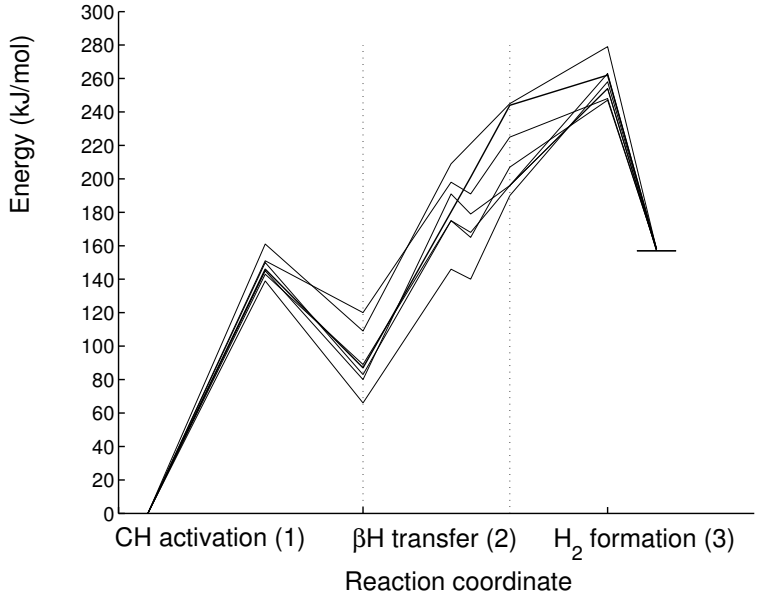

Figure 4.7: Electronic energy profiles (kJ/mol) along the reaction coordinate of the σBM/CrO mechanism for the models in Fig. 3.1.

briefly in Chapter 3 was included for clusters **H** and **I** in Fig. 3.1. This allows for relaxation of the surface through optimization of all atomic positions. For details, confer the Computational Details and Results Sections in Paper I. Here follows a brief summary of the results.

The two Cr/silica models studied by mechanical embedding both represent three-bridge chromium species, but differ in the strain exerted on the Cr–OSi bonds by the extended surface. Model **H** in Fig. 3.1, represents a relatively relaxed chromium species. This is evident from the Cr–O bond lengths of around 1.80 Å, which is similar to the bond lengths in a $Cr(OH)_3$ molecule. When forming the ethylchromium site according to reaction **1**, some relaxation of the surrounding oxide structure was found to take place. However, the surface relaxation stabilizes the product only by about 20 kJ/mol.

The transition state for the C–H/Cr–O activation step on model **H** has not been optimized at the QM-MM level. However, as obtained at the constrained cluster-model level, the Cr–O distances are close to their equilibrium values and little relaxation is expected beyond the local site. The barrier of this reaction step may thus be expected to be quite insensitive to surface relaxation, whereas the barrier against reforging a Cr–OSi bond according to reaction **3** may be underestimated by about 20 kJ/mol. For elementary steps not involving breaking of oxygen bridges, i.e. β-hydrogen transfer and C–H activation involving a Cr–OH bond, surface and bulk relaxation can be expected to be small.

Turning to model **I** in Fig. 3.1, which represents a highly strained three-bridge Cr/silica species, the surface relaxation becomes significant. For C–H activation involving cleavage of the Cr–O bond pre-stretched to 1.93 Å by the extended surface, a barrier of merely

80 kJ/mol was obtained. Again, this is an estimation based on the constrained cluster-model approach. The Cr–O bond lengths at the transition state are close to those of the unreacted model, and little relaxation is expected on the silica part. Mechanical embedding was then used to study the surface relaxation as the Cr–O bond is severed, and the results were striking. The formed silanol relaxes away from chromium, cf. Fig. 4.8. It appears that activation of strained Cr–O bonds that link chromium to the oxide support may be irreversible due to surface relaxation.

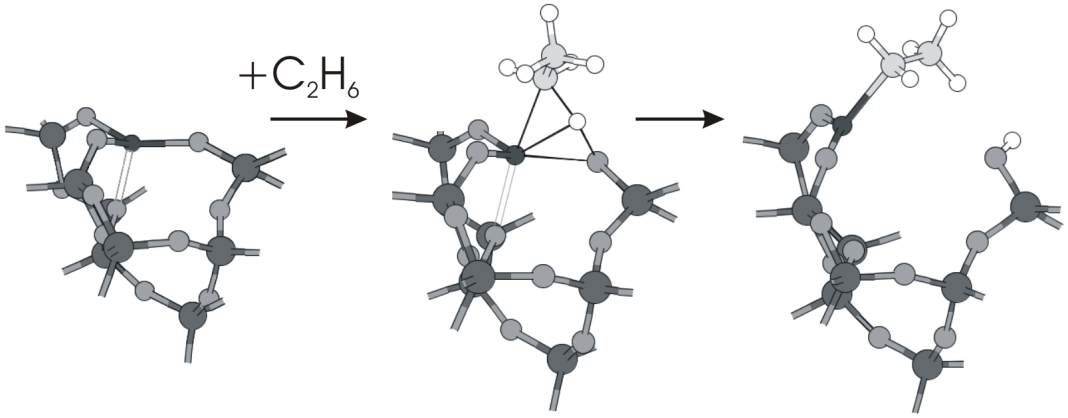

Figure 4.8: C–H activation by σ-bond metathesis at a strained three-bridge chromium species on silica gives a silanol moiety that relaxes away from chromium, thus making reformation of the Cr–O bond an unlikely event. (Figure 12 of Paper I.)

A Different Kind of Dinuclear Cr(III) Species. Preliminary Results The σBM/CrO mechanism appears energetically unfavorable due to two factors. First, C–H activation at the cost of a relatively relaxed Cr–O bond is a highly endothermic process. The product ethylchromium complex is generally 65-120 kJ/mol above the reactant asymptote of separated cluster and ethene. In addition comes the loss of translational freedom and consequent decrease in entropy pending the release of ethene at the completion of reaction **2**. The latter is a trait of the mechanism that is not affected by chromium speciation. However, if the primary product could be stabilized with respect to the unreacted site and gaseous ethane, the kinetics of the σBM/CrO mechanism would benefit. One way to achieve this is by stretching of the Cr–O bond by the extended surface. However, this appears to affect negatively the likelihood of reaction **3** (*vide supra*). Other types of species might stabilize the ethylchromium complex in different ways. In this respect, a dinuclear Cr(-O-)$_2$Cr species as represented by model **J** in Fig. 3.2 appears interesting. Here, the chromium(III) centers are linked by two oxygen bridges, thus forming a strained four-membered ring structure of Cr–O bonds. Due to localized of structural strain to the ring of Cr–O bonds, the C–H activation step will not cause relaxation beyond the local site.

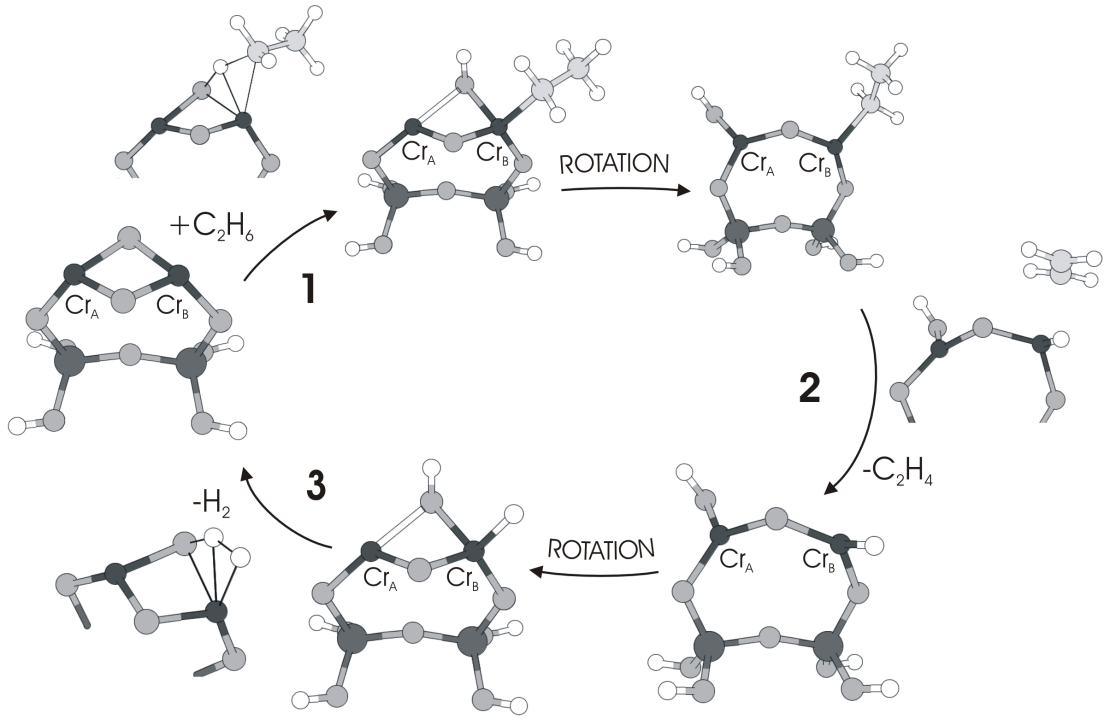

Figure 4.9: Optimized structures for a cycle of the σBM/CrO mechanism as obtained for model **J** in Fig. 3.2. The reaction steps are; (**1**) C–H activation of ethane by σ-bond metathesis at one of the Cr_A–OCr_B bonds, and subsequent rotation of the formed Cr_B-hydroxyl moiety from Cr_A, (**2**) β-H transfer to Cr_A with subsequent loss of ethene, and (**3**) rotation of the hydroxyl group from Cr_B to Cr_A, followed by Cr_A–O formation under release of H_2. Polar-covalent and dative bonds are represented by colored and blank sticks, respectively.

Computations with model **J** have been performed according to the same procedure as described in the Computational Details section of Paper I. In short, density functional theory and the BP86 [87, 88] density functional are applied as implemented in the Amsterdam Density Functional (ADF) set of programs [98].

A cycle of the σBM/CrO on the Cr(-O-)$_2$Cr site of model **J** is illustrated in Fig 4.9, and the electronic energy profile is plotted in Fig. 4.10. As shown in Fig 4.9, the initial C–H activation takes place at one of the two Cr$_A$–OCr$_B$ bonds. Structural strain is relieved, yet, the formed hydroxyl initially remains near the active chromium center. In fact, the hydroxyl ligates covalently to Cr$_A$, while the Cr$_B$–O bond becomes dative as indicated by a blank stick in Fig 4.9. A Cr$_A$(IV)-Cr$_B$(II) configuration is thus obtained, rather than the Cr$_A$(III)-Cr$_B$(III) configuration of the unreacted site; the electron spin density localized on the two chromium centers changes from about 3 e in the unreacted complex to around 2 e and 4 e on Cr$_A$ and Cr$_B$, respectively. Analogous results are presented in Paper III for the C–H activation in ethane at a Cr–OCr bond in model **D** in Fig. 3.1. However, model **D** represents a relaxed two-bridge Cr(III)OH species, and the electronic energy profile of the σBM/CrO mechanism on this model follows the general trend described above and illustrated in Fig. 4.7. On the other hand, due to strained Cr–OCr bonds in the four-membered Cr(-O-)$_2$Cr ring of model **J**, the electronic energy of C–H activation is merely 100 kJ/mol and the product ethylchromium complex lies only 7 kJ/mol above the asymptote of separated cluster model and ethane, confer the plot of electronic energy in Fig. 4.10. Furthermore, the barrier against rotation of the bridging hydroxyl away from Cr$_A$ is merely 26 kJ/mol, and the result is stabilization by another 17 kJ/mol. The electronic energy relative to the separated cluster model and ethane is thus -10 kJ/mol. The rotation is illustrated in Fig. 4.9, and plotted by a heavy line in Fig. 4.10. In the product structure, the hydroxyl has become a terminal ligand on Cr$_B$, and the Cr$_A$(III)-Cr$_B$(III) configuration is retained.

Based on the computations, the rotation step actually appears as an integral part of the σBM/CrO mechanism on the Cr(-O-)$_2$Cr species in model **J**. Conversely, if β-hydrogen transfer from the ethyl ligand to Cr$_A$ starts prior to rotation of the hydroxyl group, the Cr$_A$(III)-Cr$_B$(III) configuration is obtained before the transition state is reached, which means that the Cr$_A$–OH bond becomes dative and the Cr$_B$–OH bond becomes covalent. The dative Cr$_A$–OH bond cannot match the structural strain, the result is therefore rotation of the hydroxyl from Cr$_A$ before the β-hydrogen transfer is completed.

Subsequent to the rotation step, reaction **2** of the σBM/CrO mechanism, which consists of β-hydrogen transfer and loss of ethene, may proceed in the same fashion as described for model **A** above. Adding the ethene coordination energy of 26 kJ/mol to the reaction energy of 103 kJ/mol for β-hydrogen transfer, the electronic energy barrier of reaction **2** becomes 129 kJ/mol.

For regeneration of the Cr(-O-)$_2$Cr site according to reaction **3** the hydroxyl ligand on Cr$_B$ must first rotate back towards the hydridoCr$_A$ center, cf. Fig. 4.9. As the hydroxyl approaches Cr$_A$ the Cr$_A$(IV)-Cr$_B$(II) configuration is retained. The Cr$_A$–OH bond becomes covalent, and the Cr$_B$–OH bond becomes dative as illustrated by a blank stick in Fig. 4.9. The barrier of rotation is 46 kJ/mol, and the change in electronic energy is positive by 21 kJ/mol, cf. the heavy line in Fig. 4.10. Finally, the Cr(-O-)$_2$Cr

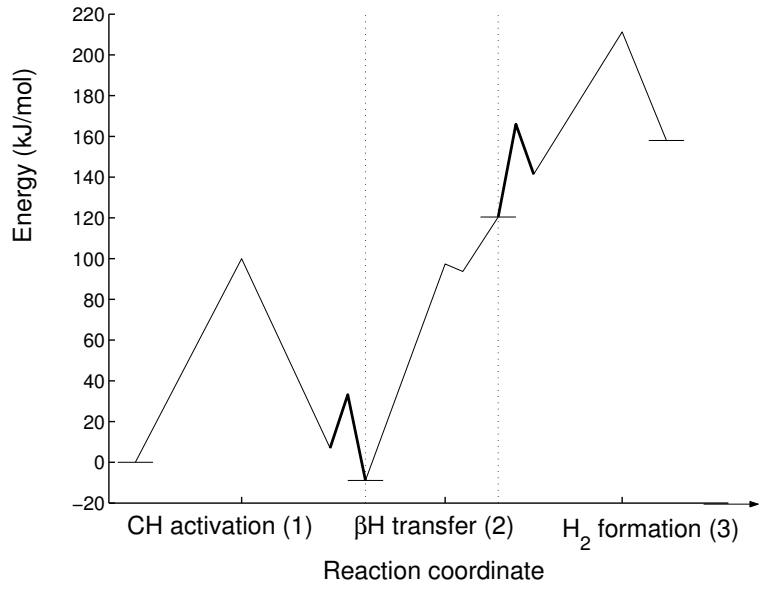

Figure 4.10: Electronic energy profile (kJ/mol) along the reaction coordinate of the σBM/CrO mechanism for model **J** as illustrated in Fig. 4.9. The reaction steps are, (**1**) C–H activation of ethane by σ-bond metathesis at one of the Cr_A–OCr_B bonds, and subsequent rotation of the formed Cr_B-hydroxyl moiety from Cr_A (heavy line), (**2**) β-H transfer to Cr_A with subsequent loss of ethene, and (**3**) rotation of the hydroxyl group from Cr_B to Cr_A (heavy line), followed by Cr_A–O formation under release of H_2.

site may reform under release of H_2. The activation energy for this step is 70 kJ/mol, and the change in electronic energy is positive by 16 kJ/mol. The total activation energy of rotation and Cr_A–OCr_B bond formation under loss of H_2 is thus 91 kJ/mol. The reaction energy is positive by 37 kJ/mol, however, the free energy change is negative due to the entropic contribution upon release of H_2 to the gas phase.

Taking into account the entropic changes upon chemisorption of ethane and subsequent desorption of ethene, reaction **2** appears rate determining for the σBM/CrO mechanism also on the Cr(-O-)$_2$Cr type of dinuclear chromium species. The activation energy for the σBM/CrO mechanism is obtained as the difference in energy of the hydridochromium complex after release of ethene, and the reactant asymptote of separated cluster and ethane. This amounts to 120 kJ/mol, which is about 80 kJ/mol lower than that obtained for any of the other models studied. However, there are some issues of accuracy, which is considered in Section 4.3 below.

Catalytic Activity of a Hydridochromium Species

C–H activation by σ-bond metathesis at a Cr–OH bond, renders a water molecule, which at typical reactor temperatures appears likely to desorb for entropic reasons (*vide supra*). Conversely, in the corresponding reaction at a strained Cr–O–M link, M being a another chromium atom, or a structural metal center of the oxide support, a hydroxyl moiety is formed and may depart from chromium. The ethylchromium site resulting from these reactions may convert to a hydridochromium complex according to reaction **2** as described above in context of the σBM/CrO mechanism. The absence of a datively bound oxygen ligand is not of consequence. Furthermore, if steam were included in the feed, which is usually not the case, the hydridochromium complex and water would most likely combine by coordination of water to chromium and formation of a Cr–OH bond according to reaction **3**. This reaction is exotherm by about 90 kJ/mol. On the other hand, dry reaction conditions may stabilize the hydridochromium complex for stoichiometric reasons. An opening is thereby made for catalytic dehydrogenation according to the σBM/CrH mechanism, which is composed of elementary reactions **4** and **2** in Fig. 4.4.

In reaction **4**, the hydridochromium complex engages in a bimolecular σ-bond metathesis reaction with a second molecule of ethane. This leads to the release of molecular hydrogen, accompanied by reformation of the ethylchromium complex. The catalytic cycle is then completed by reaction **2**; reformation of the hydridochromium complex through β-hydrogen transfer and loss of ethene to the gas phase.

The optimized structures of the transition states and reaction intermediates along the reaction coordinate of the σBM/CrH mechanism, together with a graphic representation of the changes in enthalpy and free energy, are presented in Fig. 4.11 as obtained for model **A** of a two-bridge Cr/alumina species. The catalytic cycle is also presented in the upper part of Fig. 4.6. Considering the free energy profile plotted in Fig. 4.11, C–H activation in reaction **4** appears rate determining for the catalytic σBM/CrH cycle, the activation enthalpy being 88 kJ/mol. The loss of translational freedom as ethane chemisorbs leads to a high free energy of activation of 206 kJ/mol, however, since H_2 shows no affinity toward chromium and is released to the gas phase, the reaction of C–H activation is

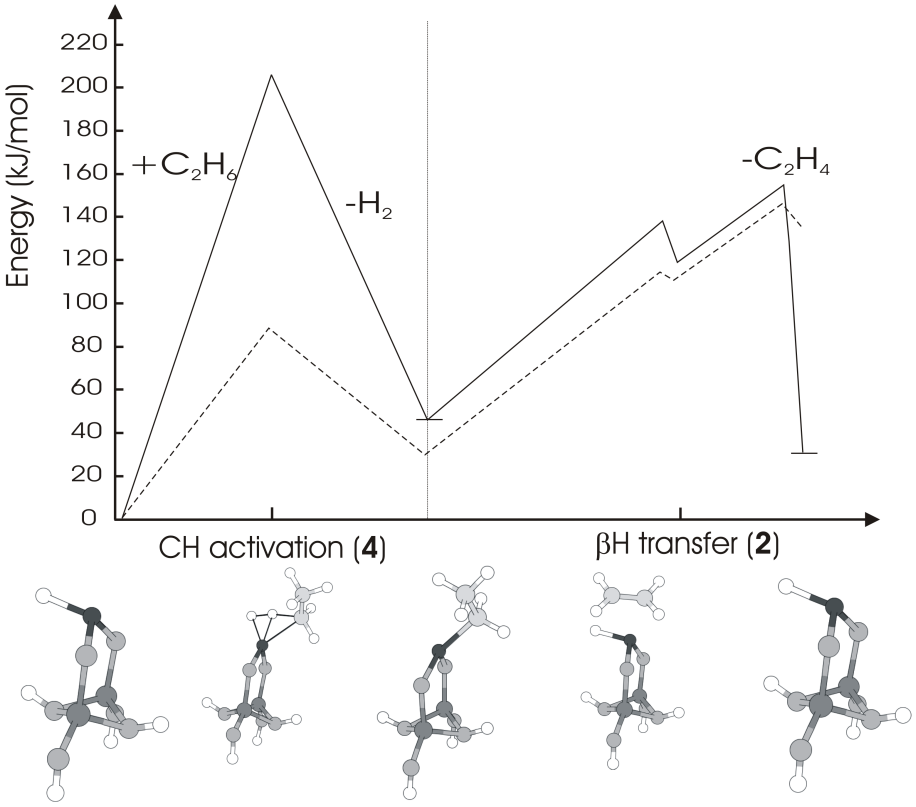

Figure 4.11: Optimized structures and plot of the changes in enthalpy (dashed line) and free energy (full line) along the reaction coordinate of the σBM/CrH mechanism on the two-bridge Cr/alumina model **A**. The thermodynamic functions are given in kJ/mol relative to that of the hydridochromium model catalyst and gaseous ethane. The reaction steps are (**4**) C–H activation of ethane with subsequent loss of H_2, and (**2**) β-H transfer to chromium with subsequent loss of ethene. (The figure is adapted from Fig. 4 of Paper III).

roughly isentropic. Furthermore, the enthalpic change for reaction **4** is only 30 kJ/mol. Reaction **2** may then proceed as described above, the free energy never exceeding the peak of reaction **1**. For a more detailed description of this catalytic cycle, see the Results sections of Papers I and III.

The Structure-Activity Relationship The gross features of the electronic energy profile along the reaction coordinate of the σBM/CrH mechanism are quite consistent with respect to chromium speciation, cf. Fig. 4.12. Taking into account the positive free energy change as ethane chemisorbs and the negative change as H_2 desorbs, reaction **4** appears rate determining for all the models studied. There are, however, some variations in activation energy depending on the nano range about chromium. In particular, the activation energy of the σBM/CrH mechanism is found to decrease with the angular strain in the link of chromium to the support, cf. Paper I. The lowest enthalpy of activation is thus obtained for the two-bridge Cr/silica model in Fig. 3.1**B**, and amounts to 71 kJ/mol. In general, the activation energies are obtained in the range of 70-110 kJ/mol, which is considerably less than that obtained for the σBM/CrO mechanism described above. In this perspective, reaction **1** appears to describe activation of a dormant chromium site and reaction **3** describes deactivation. It thus appears that the importance of the σBM/CrH mechanism relies on the ability of the site to prevent reaction **3**, which results in the formation of more stable species with chromium covalently bonded to three oxygen ligands. This ability is a sensitive function of the local structure about chromium. In particular, the species of two-bridge Cr(III)OH and strained three-bridge chromium(III) appears better adapted as precursors than the relatively relaxed three-bridge chromium species.

4.2.2 C–H Activation by Oxidative Addition

The models of mononuclear Cr(III)/silica presented in Chapter 3 have been studied with respect to C–H activation by oxidative addition as a possible route to catalytic dehydrogenation of ethane. This is the topic of Paper II, which is summarized in the following.

The reaction of C–H activation by oxidative addition at a Cr(III) center is presented schematically at the bottom of Fig. 4.2. As the C–H bond in ethane is broken, new Cr–C and Cr–H bonds are formed, thus giving an ethyl-hydridochromium(V) complex. Based on the computations, only the two-bridge CrOH species appear to support such a reaction. For the three-bridge chromium sites, the surface constraints are more severe due to the additional Cr–O ester link to the support. As a consequence, the three-bridge models do not give stable structures of the ethyl-hydridochromium(V) complex.

For the two-bridge CrOH species, a mechanism of catalytic dehydrogenation has been constructed with the initial C–H activation step proceeding by oxidative addition. Optimized structures of the stationary points of this mechanism, as obtained for model **B** in Fig. 3.1, are shown in Fig. 4.13 together with a graphic presentation of the changes

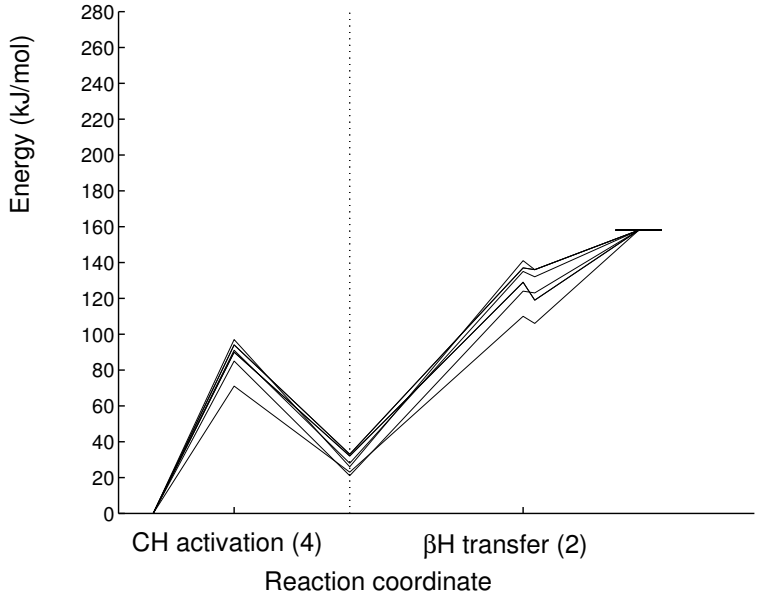

Figure 4.12: Electronic energy profiles (kJ/mol) along the reaction coordinate of the σBM/CrH mechanism for the models in Figures 3.1.

in enthalpy and free energy. Similar structures and reaction energetics were obtained for the $Cr(OH)_3$ model **E** and two-bridge Cr/silica model **F** in Fig. 3.1. For details, confer Paper II.

The C–H activation step, reaction **a** in Fig. 4.13 involves a formal double oxidation of chromium, and a Minimum Energy Crossing Point (MECP) has been located on the seam between the quartet-spin potential-energy surface of Cr(III) and the doublet-spin potential-energy surface of Cr(V). Subsequent to the change of spin state, the C–H activation path passes through a transition state on the spin doublet potential energy surface, leading to the formation of a highly unstable ethyl-hydridochromium(V) complex. The computed activation barrier for breaking the C–H bond is in excess of 150 kJ/mol. However, to prevent the reverse reaction, β-hydrogen transfer to complete the catalytic cycle must take place in the extension of the C–H activation step. This involves a stereochemical rearrangement of ligands in the ethylhydridochromium(V) complex, cf. reaction **b** in Fig. 4.13. The bottleneck of C–H activation is therefore better represented by the transition state of ligand rotation. Furthermore, considering the free energy profile in Fig. 4.13, this step appears to be rate determining for the overall dehydrogenation process, and the computed enthalpy and free energy of activation are ca. 220 and 350 kJ/mol, respectively.

Subsequent to stereochemical rearrangement, a β-hydrogen of the ethyl group may, assisted by agostic interaction, transfer to the hydride ligand as illustrated in reaction **c** of Fig. 4.13. Gaseous H_2 is formed, leaving a chromium(V) cyclopropane surface complex in which ethylene is di-σ bonded to chromium. Finally, in reaction **d** of Fig. 4.13, spin flip of chromium *d* electrons leads to reformation of the original spin-quartet CrOH species with a π-bonded ethene ligand. Driven by the entropic contribution to the free energy,

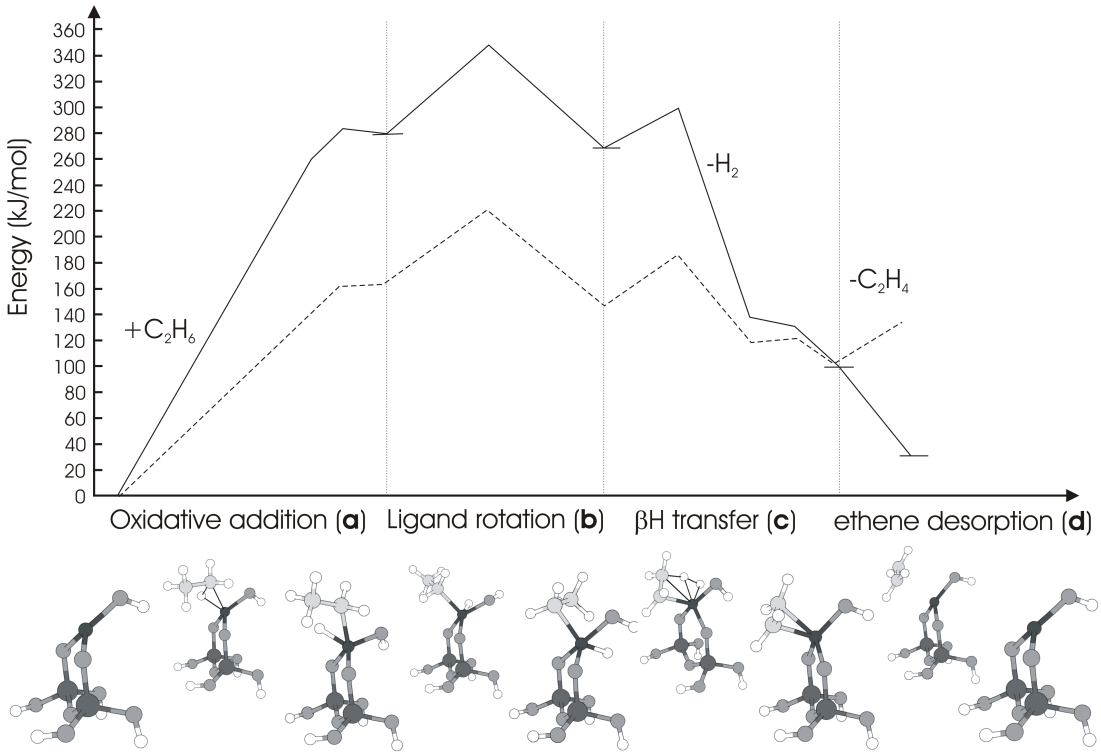

Figure 4.13: Optimized structures and plot of the changes in enthalpy and free energy along the reaction coordinate of catalytic dehydrogenation following C–H activation by oxidative addition on model **B** in Fig. 3.1. The thermodynamic functions are given in kJ/mol relative to that of the hydridochromium model catalyst and gaseous ethane. The reaction steps are (**a**) Oxidative addition of ethane, (**b**) stereochemical rearrangement, (**c**) β-hydrogen transfer to hydride with subsequent loss of H_2, and (**d**) Spin-flip of the chroma(V)cyclopropane complex, with subsequent loss of C_2H_4 to the gas phase. (The figure is adapted from Fig. 6 of Paper II.)

ethene desorbs thus completing the catalytic cycle.

Oxidative Addition v/s σ-Bond Metathesis

Compared to the mechanisms of catalytic dehydrogenation that are based on C–H activation by σ-bond metathesis, the rotation segment of the C–H activation step by oxidative addition puts severe constraints on the angular momentum of the reacting alkane molecule. Moreover, oxidative addition appears restricted to CrOH moieties bonded to the surface *via* two oxygen bridges. Based on the thermodynamic parameters, this type of surface site favors the σBM/CrH mechanism based on C–H activation by σ-bond metathesis at a hydridochromium complex. The computed activation energy of this mechanism is on the order of 100 kJ/mol, compared to 220 kJ/mol obtained for the mechanism based on C–H activation by oxidative addition. It thus appears that C–H activation by oxidative addition is an unlikely route to catalytic dehydrogenation on Cr(III).

4.3 Is the Computational Model Trustworthy?

The computational model includes clusters to represent surface sites on oxides, and density functional theory to describe reactions on transition metal centers. Some assessment of accuracy is necessary.

The Cluster-Model Approach Based on the QM-MM computations presented in Paper **1**, structural constraints of the encapsulating surface have little effect on the energy barriers obtained for the relatively relaxed chromium surface species. However, the long range electrostatic potential is not included in the quantum chemical description of the active site. Furthermore, there may be effects that are only captured by expanding the region described at the quantum mechanical level. In the Discussion section of Paper III, the use of cluster models is defended as follows.

Support of the smaller cluster models is found in the reproducibility of reaction energy profiles of the σBM/CrO and σBM/CrH mechanisms from the simplest $Cr(OH)_3$ model to the more sophisticated models. Similarly, in a computational study of ethene metathesis over Mo/alumina, the reaction barrier was found to remain stable over a range of cluster sizes [64]. Furthermore, Kubicki and Apitz [63] and De Vito *et al.* [65] report that small alumina clusters terminated by OH or HOH groups, are adequate for describing adsorption and chemisorption over alumina surfaces.

Neglect of the long-range Madelung field in the models of Cr/alumina may be defended based on studies of water adsorbing and dissociating on the surface of alumina. Initiation of the σBM/CrH mechanism requires that water desorbs after being formed by C–H activation involving a Cr–OH bond. The Madelung field has been shown to contribute about 20 kJ/mol to the adsorption energy of molecular water on surface aluminum ions of alumina [126,127]. While this appears to be an upper limit to what might be expected for the coordination energy of water on CrO_x species dispersed on alumina, it would still leave the free energy of desorption of water negative by 30-50 kJ/mol at 500°C. Concerning activation energies, it is instructive to consider dissociation of water

on Al–O pairs on models of alumina surfaces. This may be considered as a high-polarity analogue of reaction **1** in Fig. 4.3, thus presenting a worst-case scenario. Inclusion of the Madelung field was found to destabilize the energy of the dissociative product by about 20 kJ/mol relative to the reactant asymptote [126, 127]. Although the neglect of the long-range potentials may be expected to impart notably smaller errors than this to the computed energy profiles for the σBM/CrH and σBM/CrO mechanisms, discussion has been restricted to energy differences larger than 20 kJ/mol.

Density Functional Theory The results presented above are based on Density Functional Theory (DFT) and the BP86 density functional [87, 88] as implemented in the ADF set of programs [98]. In a preliminary assessment of the accuracy of the method, the electronic activation energies of the σBM/CrO and σBM/CrH mechanisms have now been investigated using three additional methods. These are: (i) Multi-Configuration Self-Consistent Field (MCSCF) with the three unpaired α electrons on chromium(III) in an active space of ten orbitals, and the dynamical correlation energy estimated by perturbation theory to the second order, MCQDPT2 [79], (ii) Restricted Open shell Hartree Fock (ROHF) with correlation energy estimated by second order perturbation theory, MP2 [77], and (iii) Density Functional Theory (DFT) using the B3LYP [89] hybrid density functional. Brief descriptions of these different methods are given in Chapter 2. The MCQDPT2 computations were performed with Gamess [128], while the MP2 and the B3LYP computation were performed using the Gaussian set of programs [129]. The basis set chosen for all these computations was the TZV1P basis set described in Ref. [130]. It is of triple-zeta valens (TZV) quality with a polarization function on hydrogen and oxygen. This is comparable to the basis set used in the BP86 computations as described in Paper I.

Due to the small size, the $Cr(OH)_3$ model in Fig. 3.1**E** is well suited for all three of the additional computational methods. In addition, model **B** which represents a two-bridge Cr/silica species, has been studied at the MP2 and B3LYP levels. For model **J** in Fig. 3.2, which represents a dinuclear chromium species with chromium centers linked by a double oxygen bridge, the activation energy of the σBM/CrO mechanism is considered using B3LYP. For all three models, single-point computations have been performed using the geometries optimized at the BP86 level.

Consider first the σBM/CrO mechanism. β-hydrogen transfer with subsequent desorption of ethene is found rate-determining, the electronic energy of activation being obtained as the change in electronic energy moving from separated cluster model and ethane, to hydridochromium and ethene. As computed with BP86, this amounts to 196 kJ/mol for the $Cr(OH)_3$ model, while somewhat lower barriers of 177, 170, and 165 kJ/mol are obtained with the B3LYP, MP2, and MCQDPT2 methods, respectively. For model **B**, the activation barrier of the σBM/CrO mechanism, with C–H activation taking place at one of the Cr–OSi bonds, is obtained as 225 kJ/mol using the BP86 functional. Computed both at the B3LYP and the MP2 levels, an activation energy of 208 kJ/mol is obtained. Based on these computations the activation energy of the σBM/CrO mechanism reported in Papers I and III, appears to be somewhat higher than the real value.

The electronic energy barrier of the σBM/CrO mechanism on the Cr(-O-)$_2$Cr ring structure in model **J**, as illustrated in Fig. 4.9, is obtained at merely 120 kJ/mol using the BP86 functional. The same value is actually obtained when using B3LYP to compute the change in electronic energy going from separated cluster and ethane to hydridochromium and ethene. However, B3LYP predicts the C–H activation step, rather than the desorption of ethene, to be rate determining for the σBM/CrO cycle on the Cr(-O-)$_2$Cr ring structure. A C–H activation barrier of 137 kJ/mol is obtained using B3LYP, whereas a barrier of 100 kJ/mol was computed with BP86. The identity of the rate-determining step for the σBM/CrO mechanism on model **J** is therefore uncertain at this point, although, the activation energy appears quite consistent at 130$\pm$10 kJ/mol. It should also be noted that the interaction between Cr_A(III)-Cr_B(III) and Cr_A(IV)-Cr_B(II) configurations involved in the σBM/CrO mechanism on model **J** is not explicitly taken into account by the DFT single-determinant descriptions. A multiconfiguration wavefunction approach is therefore suggested for further studies.

Turning to the σBM/CrH mechanism, the activation energy of the catalytic cycle is obtained as the barrier of C–H activation in ethane at the hydridochromium complex. The barrier of 107 kJ/mol predicted by BP86 for the reaction on the Cr(OH)$_3$ model is the upper bound obtained for the set of cluster models. Due to difficulties in determining the multi-configurational electronic state at the transition state of C–H activation, a MCQDPT2 energy has not been obtained. Based on B3LYP and MP2 computations the activation energy of the σBM/CrH mechanism on the Cr(OH)$_3$ model is predicted at 138 and 120 kJ/mol, respectively. For model **B**, the activation energy is obtained as 71, 97, and 78 kJ/mol using the BP86, B3LYP, and MP2 methods, respectively. It thus appears that the activation energy of the σBM/CrH mechanism may be somewhat higher than that predicted based on the computations with the BP86 functional. However, the magnitude still appears on the order of 100 kJ/mol.

Although a more thorough investigation should be performed to obtain accurate energy barriers, this preliminary assessment indicates that the qualitative conclusions made in Papers I and III are robust with respect to the computational method.

4.4 Summary of the Computational Results

By means of density functional theory and a cluster-model approach, we have investigated models of Cr(III) on alumina, silica and chromia supports with respect to activity in the catalytic dehydrogenation of ethane. Mechanisms have been constructed based on the assumption that the C–H activation step proceeds by σ-bond metathesis or by oxidative addition involving a single chromium center. From the study of mononuclear Cr(III)/silica, reported in Papers I and II, σ-bond metathesis appears as the favored route to catalytic dehydrogenation. Furthermore, the results presented in Paper III indicate that this type of catalytic activity depends on the local structure around chromium, rather than the choice of oxide support.

For models of Cr(III) linked by three oxygen bridges to metal ions of the oxide support or to neighbor chromium atoms, a reaction mechanism consisting of the following

three steps is found viable: **1** C–H activation of ethane according to σ-bond metathesis accompanied by cleavage of a Cr–O bond and formation of O–H and Cr–C bonds, **2** β-H transfer to chromium with subsequent loss of ethene, and **3** regeneration of the chromium site by means of σ-bond metathesis with subsequent loss of H_2. The catalytic cycle composed of these three steps is referred to as the σBM/CrO mechanism and is illustrated in Fig. 4.6. Apart from the absence of molecular adsorption of ethane, the mechanism agrees with a proposal in the literature [3].

For the σBM/CrO cycle with the initial C–H activation step involving a relatively relaxed Cr–O bond, free-energy calculations presented in Papers I and III indicate desorption of ethene in reaction **2** as the rate-determining step. On chromium species with three oxygen bridges to the support, the free energy and enthalpy of activation are obtained in excess of 300 and 200 kJ/mol, respectively. On the other hand, as reported in Section 4.2.1 above, a significantly lower activation energy is obtained for the σBM/CrO mechanism on a dinuclear $Cr(\text{-}O\text{-})_2Cr$ ring structure with chromium centers linked by two somewhat strained oxygen bridges. Although the rate-determining step in this case remains uncertain due limitations of the computational method, the activation energy appears quite consistent around 130 kJ/mol. This lower activation energy is due to release of structural strain upon C–H/Cr–O activation in reaction **1**. However, the strain also gives rise to two extra reaction steps in the catalytic cycle, cf. Fig. 4.9. The hydroxyl moiety formed in reaction **1** relaxes away from the active chromium center prior to reaction **2**, and must subsequently rebound for the completion of reaction **3**.

Based on the computations, an alternative mechanism is found energetically favorable in which C–H activation takes place at the reactive hydridochromium complex formed in reaction **2** above, rather than at more stable chromium species with three oxygen ligands. The catalytic cycle, referred to as the σBM/CrH mechanism, is illustrated in Fig. 4.6. The initial products of the C–H activation step are ethylchromium and gaseous H_2. The hydridochromium site is then reformed by β-hydrogen transfer according to reaction **2**. C–H activation is found rate determining of this two-step cycle, and the computed enthalpy of activation is obtained on the order of 100 kJ/mol.

Although the activation energy of the σBM/CrH mechanism appears relatively low, any catalytic activity along this route depends on the stabilization of a reactive hydridochromium site, i. e. the ability of the site to prevent formation of more stable species in which chromium is covalently bonded to three oxygen ligands. This ability is a sensitive function of the nano-range surroundings of chromium. On two-bridge CrOH species, a water molecule is formed by initial C–H activation involving cleavage of a Cr–OH bond. Desorption appears likely for entropic reasons, and stabilizes the hydridochromium site stoichiometrically. Conversely, activation at a chromium species with three Cr–O links to the surface renders a surface-bound hydroxyl moiety instead of water. At strained surface sites, this hydroxyl may relax away from chromium, which hinders reformation of the Cr–O bond. On the other hand, with the hydroxyl moiety remaining close to chromium, fast regeneration of the Cr–O bond is to be expected according to reaction **3** as described above.

Regarding the role of the oxide support, it is concluded in Paper III that the same type of chromium species may be active on alumina, silica, and chromia, and act according to

the same reaction mechanism. For effective catalysis it appears that the oxide support should sustain reactive structures, such as the hydridochromium species and the strained $Cr(\text{-}O\text{-})_2Cr$ ring structure, by preventing reorganization to the more stable three-bridge chromium species.

4.5 Theory and Experimental Data in Concert?

The computational results summarized above are to be seen against a background of more than 70 years of experimental observations. The following is a summary of the Discussion sections of Papers I and III. The computational results and experimental data from the literature are discussed with respect to (i) the mechanism of catalytic dehydrogenation, (ii) the relationship between activity and chromium speciation, and (iii) the role of the oxide support.

The Mechanism of Catalytic Dehydrogenation Based on the computations, the σBM/CrH mechanism with activation energy around 100 kJ/mol appears as an energetically favorable route to catalytic dehydrogenation on Cr/oxide catalysts. Although this mechanism relies on the survival of a highly reactive hydridochromium complex, there are several observations that indicate it may be possible. Chromium hydrides have been observed on chromia treated with H_2 [131], hydridochromium complexes have been synthesized [125], and there is evidence of C–H activation of ethane over silica-supported transition metal hydrides, including chromium hydride [132–134]. Still, certain details of the catalyst preparation or reaction conditions may result in destabilization of the hydridochromium sites in favor of the more stable chromium complex with three ligands covalently bonded through oxygen. For instance, this appears likely in the presence of moisture, which may remain on the catalyst surface after reduction, or be included in the feed. Furthermore, in paper IV of this thesis, the $Cr(\text{-}O\text{-})_2Cr$ ring structure is found to react exothermically with water to give a dinuclear site of two-bridge CrOH species. It thus appears that catalytic dehydrogenation under moist conditions relies on the σBM/CrO mechanism and suffer a relatively high activation energy. In support of these ideas, it has been reported that catalytic dehydrogenation is poisoned by even small amounts of moisture in the feed [16, 17].

The existence of more than one mechanism, possibly involving different types of chromium species, seems to be indicated by the wide range of activation energies that have been reported for the catalytic dehydrogenation reaction. For the dehydrogenation of ethane over Cr/silica, Lugo and Lunsford reported an activation energy of 117 kJ/mol, which might indicate activity due to the σBM/CrH mechanism on two-bridge chromium and/or the σBM/CrO mechanism on $Cr(\text{-}O\text{-})_2Cr$ ring structures. On the other hand König and Tétényi [14, 15] obtained an activation energy of 180 kJ/mol over α-chromia, which might indicate activity due to the σBM/CrO mechanism on three-bridge chromium species. Furthermore, DeRossi *et al.* [17] obtained activation energies in the range of 60-100 kJ/mol for the dehydrogenation of propane over Cr/alumina, Cr/silica, and chromia, while Airaksinen *et al.* [47] reported a somewhat higher barrier of about 140 kJ/mol for

the dehydrogenation of iso-butane over Cr/alumina. However, alkanes of more than two carbon atoms may be dehydrogenated along reaction paths that are closed to ethane.

The rate-determining step of catalytic dehydrogenation is another useful parameter in the comparison of computational and experimental results. Proposals in the literature based on experimental observations include both C–H activation [47] as obtained the for the σBM/CrH mechanism on two-bridge chromium, and desorption of alkene [14, 135] as obtained for the σBM/CrO mechanism on three-bridge chromium. However, by combining isotope labelling and transient reactions, Olsbye *et al.* [59] recently distinguished C–H activation as the likely rate-determining step in the catalytic dehydrogenation of ethane over a Cr/alumina catalyst.

Yet another approach to investigate the mechanism of catalytic dehydrogenation is related to the C–H activation step, which in the modelled σBM/CrH and σBM/CrO mechanisms involves the cleavage of a Cr–O bond and a C–H bond, respectively. A common idea in the literature is that the catalytic cycle of dehydrogenation involves C–H activation at a Cr–O pair [3, 17, 47, 54]. The possibility of this idea is indicated by the detection of hydridochromium and surface hydroxy groups by IR after hydrogen flow over chromia [131]. Furthermore, poisoning of Cr/zirconia catalyst by K^+ has been argued due to blocking of oxygen atoms near chromium, thus preventing C–H activation [136]. On the other hand, rearrangement of a Cr/alumina surface has been observed upon exposure to dehydrogenation conditions [17], which may indicate irreversible loss of Cr–O bonds, preventing reaction **3** in Fig. 4.1.

In an effort to determine the role of oxygen ligands to chromium, Puurunen *et al.* [25] performed dehydrogenation experiments with chromium deposited on alumina surfaced by aluminum nitride. While the replacement of oxygen by the more basic nitrogen was expected to increase the probability of dissociation of the alkane, and thereby the rate of dehydrogenation, the opposite was found. The authors concluded that nearby oxygen may be required to obtain chromium sites with high activity. As an alternative explanation, we suggest in Paper I that in the dominant catalytic cycle of elementary reactions, C–H activation does not involve a structural anionic ligand, but rather a hydride. In this case the vicinity to chromium of the ligand–H group formed in reaction **1** will determine the activity as the hydride is easily consumed in reaction **3** unless the ligand–H group is removed from chromium. In turn, this may lend support to the σBM/CrH mechanism and the notion that precursor surface species are activated by reaction **1**.

The Active Chromium Species Based on the computed activation energies, it appears that efficient catalysis might be related to the ability of the surface sites to stabilize the hydridochromium complex. In this respect, the two-bridged CrOH species that was proposed by DeRossi *et al.* [17] appears as a favorable precursor. The formation of CrOH surface species have actually been observed by infra-red spectroscopy on Cr/alumina during pre-reduction with H_2 [33]. Water is formed in the reaction, then adsorbs and dissociates on the surface [17, 21, 33, 47]. However, the presence of water may terminate the σBM/CrH mechanism, which would explain the relatively low activity obtained for H_2-reduced catalysts [21, 47]. As mentioned above, even a small amount of water in the feed has been found to poison catalytic dehydrogenation [16, 17]. On the other hand, one

obtains higher catalytic activity by submitting the calcined catalyst to dehydrogenation without pre-reduction by H_2 [25, 47]. In this case, the catalytic activity increases during time on stream together with continued release of water after CO_x reduction products are no longer observed [25, 47, 137]. This apparent correlation between desorption of water from the catalyst surface and increase in catalytic activity, might signify activation of the σBM/CrH mechanism at CrOH species according to reaction **1** in Fig 4.6. On the other hand, the increase in activity during time on stream has been proposed due to catalytic dehydrogenation on coke which is deposited on the surface [138]. However, in a recent contribution by Olsbye *et al.* [59], the latter explanation was found unlikely based on studies of ethane dehydrogenation over Cr/alumina by isotope labelling and transient reactions.

Based on the computations summarized in Section 4.4 above, both CrOH and Cr(-O-)$_2$Cr species appear as possible precursors to the catalytically active species. In this respect, interesting results are presented in Paper IV of this thesis, and are summarized in Chapter 5. The reaction steps leading to the active Cr/silica catalyst have been studied by means of cluster models and density functional theory. In agreement with the proposals of DeRossi *et al.* [17] and Wittgen *et al.* [111, 112], respectively, both CrOH and Cr(-O-)$_2$Cr species are obtained as catalyst precursors.

Role of the Oxide Support The catalytic activity of chromium with respect to dehydrogenation is reported to depend on the choice of oxide carrier as Cr/zirconia > Cr/alumina > Cr/silica > α-chromia [17, 20, 26–28]. However, there appears to be a consensus in the literature that the role of the support is primarily one of stabilizing the reactive chromium species or its precursor. In Paper III a conclusion to this effect is made by pointing to the favorable energetics of the σBM/CrH mechanism on two-bridge chromium and the stability of the reaction energy profile with respect to change of oxide support. It is further argued that a successful support should prevent the surface species from reorganizing to structures where chromium is anchored to the oxide support by three or more oxygen bridges. In this respect, silica and alumina differ. On silica, chromium aggregates more easily into crystallites of α-chromia [27, 30, 37, 52, 139], which leaves fewer chromium atoms exposed. Furthermore, of those that are exposed a considerable fraction is likely to be anchored by more than two oxygen bridges. Alumina, on the other hand, is able to stabilize a layer of amorphous chromia even beyond monolayer loading of chromium [18, 20, 22, 27]. Actually, based on the results in Paper III it appears that the formation of polynuclear chromium species may be advantageous if this increases the number of surface chromiumhydroxyls that may become activated. Furthermore, the results presented in Section 4.2.1 above indicate that two-bridge dinuclear Cr(-O-)$_2$Cr species may also be active in catalytic dehydrogenation. In line with these results, Puurunen *et al.* [24] have reported that mononuclear Cr/alumina is less active than polynuclear Cr/alumina. This observation is consistent with a beneficial interaction between chromium centers to prevent chromium(III) ions from forming three-bridge chromium species in octahedral vacancies in the alumina surface.

Summary The computational results summarized in Section 4.4 above have been discussed with respect to experimental observations reported in the literature. Subject to discussion there are indications that theory and experimental data are in agreement, albeit, definite conclusions cannot be made. In Chapter 7 of this thesis summary, an experiment is proposed which may give information regarding the dominant mechanism of catalytic dehydrogenation, and in turn provide an indication regarding the structure of the active chromium species.

Chapter 5

Modelling of Catalyst Precursors

One approach to investigate the local environment of catalytically active Cr(III) ions is by starting with the surface in a well characterized initial state, and studying the reaction steps leading to an active catalyst. This is the idea behind the computational study presented in Paper IV of this thesis and summarized below.

The computations are based on an interesting experiment performed by DeRossi *et al.* [17] to clarify the role of oxidation states +II and +III in catalytic dehydrogenation. A Cr/silica catalyst of 0.5 wt% chromium was prepared by calcination with O_2 and subsequent reduction with CO, thus leaving chromium mainly in the +II oxidation state. The catalyst sample was then either submitted directly to dehydrogenation, or pre-heated with water thus selectively oxidizing Cr(II) to Cr(III). In the latter case, catalytic dehydrogenation in absence of Cr(II) was taken as evidence of active Cr(III). Furthermore, DeRossi *et al.* [17] reported near identical IR spectra of CO probe molecules adsorbed on the Cr(III)/silica species that were obtained stepwise through reduction by CO and oxidation by water, as on those obtained directly through reduction with H_2. Moreover, Hakuli *et al.* [52] later reported the same extent of reduction of calcined Cr/silica surfaces with H_2 as with iso-butane as reducing agent. These findings indicate that on silica supports similar Cr(III) species are formed by oxidation of Cr(II) with water as by reduction of high-valent chromium species by H_2 or by alkane. Furthermore, Hakuli *et al.* [52] reported equal catalytic activity of the H_2-reduced catalyst as after leaving the calcined catalyst 5 min on stream with i-butane. It thus appears that the Cr(III)/silica species that are formed through oxidation of Cr(II)/silica with water are candidates for the catalytically active site on Cr/oxide catalysts referred to as *redox Cr(III)*, and described as Cr(III) species resulting from the reduction of high-valent chromium [17,19–21,26,56,57].

A computational study of reaction paths for the oxidation of Cr(II)/silica by water, and investigation of the product Cr(III) species with respect to activity in catalytic dehydrogenation, may give some insight to the structural properties of active chromium, and, furthermore, clarify the role of redox history of the active site. Paper IV of this thesis, summarized below, concerns the oxidation reaction with water. Possible catalytic activity of the product Cr(III) species has been investigated in Paper III and in Chapter 4 of this thesis summary.

5.1 Oxidation of Cr(II)/silica by Water

In the experimental setup of DeRossi *et al.* [17] a 0.5 wt% Cr/silica catalyst was used. For Cr/silica surfaces with chromium load below 2 wt%, experimental evidence indicates that species of mononuclear Cr(II) are dominant after reduction of the calcined catalyst by CO [32, 116, 117]. This defines the starting point of the computations in Paper IV. Using the three cluster models of Cr(II)/silica in Fig. 3.4, reaction schemes have been investigated that are based on dimerization of mononuclear Cr(II) prior to the oxidation step. This is in accordance with suggestions by Groeneveld *et al.* [34]. Based on the computations, it appears that hydrolysis of Cr(II)–OSi bonding gives a chromium(II)hydroxyl and a silanol moiety, Cr(II)OH and SiOH. The Cr(II)OH moiety becomes mobile on the surface, and oxidation to Cr(III) takes place in the encounter between two Cr(II)OH moieties. The results are described in detail in Paper IV. Here is presented a brief summary.

Formation and Mobility of Cr(II)OH on the Surface of Amorphous Silica Figure 5.1 shows **a** the hydrolysis of a Cr–OSi bond in a mononuclear Cr(II) species, and **b** a mechanism by which the product Cr(II)OH moiety might transfer from one silicon tetrahedron to another on the surface of amorphous silica. In reaction **a**, hydration of the chromium center, with subsequent hydrolysis of the Cr–OSi linkage and rotation of the singly linked Cr(II)OH moiety, is completed without activation energy. The Cr(II)OH moiety is thus free to react with surface species in its immediate surroundings. Reaction with a surface siloxane is found leading to transfer of chromium to another silicon tetrahedron. This is illustrated in reaction **b** in Fig. 5.1. Here a cluster model is used which incorporates larger parts of the silica surface. If the Cr(II)OH moiety of structure $\mathbf{A}_3$ in Fig. 5.1**a** rotates and coordinates to a nearby siloxane, a surface species as represented by structure $\mathbf{B}_1$ in Fig. 5.1 may be obtained. Next, the oxygen that links the Cr(II)OH moiety to the surface, O_A in the figure, coordinates to a nearby silicon, Si_B, which becomes five-coordinated, cf. structure $\mathbf{B}_2$ in Fig. 5.1. The computed activation energy of this step is merely 2 kJ/mol, and the change in energy is -18 kJ/mol. A small barrier of 11 kJ/mol is then surmounted as a synchronized shift of Cr–O and Si–O bonds results in the formation of a new covalent Si_CO_B–Cr bond, while the original Cr–O_ASi_A bond becomes dative. The CrOH moiety has thus shifted from one silicon tetrahedron to another. This is accompanied by rupture of the six-atom siloxane ring in structure $\mathbf{B}_1$ in favor of the eight-atom ring in structure $\mathbf{B}_3$. The change in electronic energy for the final step is -32 kJ/mol. The electronic activation energy for reaction **b** is merely 2 kJ/mol and the total energy change is -50 kJ/mol. In general, the activation energy appears to depend on the relative ring-strain of the siloxane rings that are broken and formed in the reaction. For instance rupture of the six-atom siloxane ring in $\mathbf{B}_1$ in favor of the eight-atom ring in $\mathbf{B}_3$, is accompanied by the release of 50 kJ/mol, while for the reaction path traversed in the opposite direction, this energy would enter into the activation energy.

By rotation of the CrOH moiety in structure $\mathbf{B}_3$ from the O_A siloxane to another siloxane, and repetition of the reaction steps presented in Fig. 5.1**b**, the CrOH moiety may continue its travel across the silica surface.

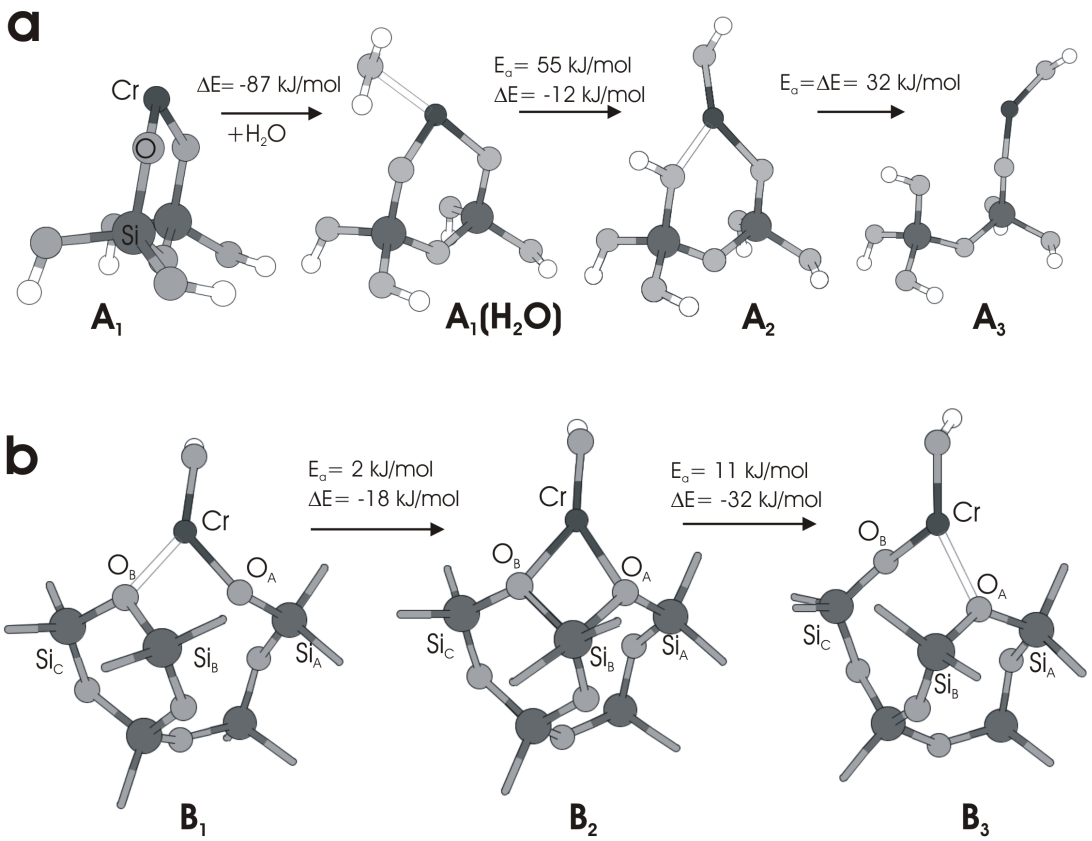

Figure 5.1: Optimized stationary structures and electronic energies for the reaction steps leading to relocation of chromium on a silica surface. The main reaction steps are: **a** Hydration of chromium followed by hydrolysis of a Cr–OSi bond by σ-bond metathesis, and rotation of the CrOH moiety from the silanol group. **b** The CrOH moiety moves from one silicon tetrahedron to another *via* a structure involving a five-coordinated silicon center. For each reaction step in the figure, E_a represents the electronic energy of activation and ΔE is the change in electronic energy. (The figure is adapted from Fig. 2 of Paper IV.)

Oxidation of Cr(II) to Cr(III) Oxidation is found to take place in the encounter between two Cr(II)OH moieties. An overview of the obtained theoretical models of reaction paths is illustrated in Fig. 5.2. Starting from two non-interacting Cr(II)OH moieties in structure $\mathbf{C}_0$, three reaction paths of oxidation have been found, all leading to structure **G** in Fig. 5.2 which is characterized by two oxo-linked Cr(III)OH moieties.

The initial interaction involves the empty *d*-orbitals of the chromium(II) centers and the non-bonding electrons of the hydroxyl ligands. This appears to give two interchangeable structures, $\mathbf{C}_1$ or $\mathbf{C}_2$ in Fig. 5.2, which differ in the interaction involving one or two hydroxyls. The electronic energies relative to $\mathbf{C}_0$, are -122 and -99 kJ/mol, respectively. Furthermore, the covalent Cr–O–Cr link in structure $\mathbf{C}_3$ in Fig. 5.2, results from an energy-neutral condenzation reaction of the hydroxyl groups in $\mathbf{C}_2$. Based on the computations, it appears that structures $\mathbf{C}_{1-3}$ may exist in a dynamic equilibrium.

The next step is oxidation, and minimum energy crossing points [101, 102] have been located on the seam between the nonet spin potential energy surface of the dinuclear $\mathbf{C}_{1-3}$ species and the septet spin potential energy surface of the oxidized products. Starting from $\mathbf{C}_1$ or $\mathbf{C}_3$, one of the two chromium centers is found to be formally oxidized from +II to +IV. The activation energies of oxidation are 155 and 117 kJ/mol relative to the energy of $\mathbf{C}_1$ and $\mathbf{C}_3$, respectively. On either reaction path, subsequent rearrangement of covalent bonds results in oxidation state +III on both chromium centers. The structures labelled **H** and **E** in Fig. 5.2 are obtained. See Paper III for a detailed description of the elementary reaction steps that are involved. Structure **H** is a dinuclear Cr(III) species with a hydridoCr(III) and a hydroxoCr(III) moiety linked by a single oxygen bridge. In structure **E**, which is formed by loss of a H_2 molecule to the gas phase, the Cr(III) centers are connected by a double oxygen bridge. Relative to the non-interacting Cr(II)OH moieties in $\mathbf{C}_0$ the change in electronic energy in forming structures **H** and **E** is -136 and -102 kJ/mol, respectively. Furthermore, starting from structure $\mathbf{C}_2$ in Fig. 5.2, both chromium centers are oxidized in a single reaction step resulting directly in structure **H** in Fig. 5.2, the activation energy being 130 kJ/mol.

Through reaction of a water molecule with structures **H** or **E** the thermodynamic product of the reaction is obtained, cf. structure **G** in Fig. 5.2. This is a dinuclear chromium species with two oxo-linked Cr(III)OH centers, each chromium being anchored to silica *via* a third oxygen ligand. The total change in electronic energy for the reaction from structure $\mathbf{C}_0$ to **G** is -228 kJ/mol.

The oxidation step appears rate determining for each of the reaction paths in Fig. 5.2 from structure $\mathbf{C}_0$ *via* structures $\mathbf{C}_{1-3}$ to **G**. Relative to the energy of the two non-interacting Cr(II)OH moieties in structure $\mathbf{C}_0$, the activation energy is obtained as 33, 31, and 17 kJ/mol along the reaction paths *via* $\mathbf{C}_1$, $\mathbf{C}_2$, and $\mathbf{C}_3$ respectively. This span of activation energies falls inside the error bars of the computational model. The three different routes are therefore not distinguishable at this point. However, each of the reaction paths lead to the same product structure **G**.

In summary, the total activation energy obtained for the dimerization of Cr(II) and subsequent oxidation to Cr(III) is of the order of 50 kJ/mol, and the total change in electronic energy is of the order of -200 kJ/mol. Admittedly, some uncertainty in these

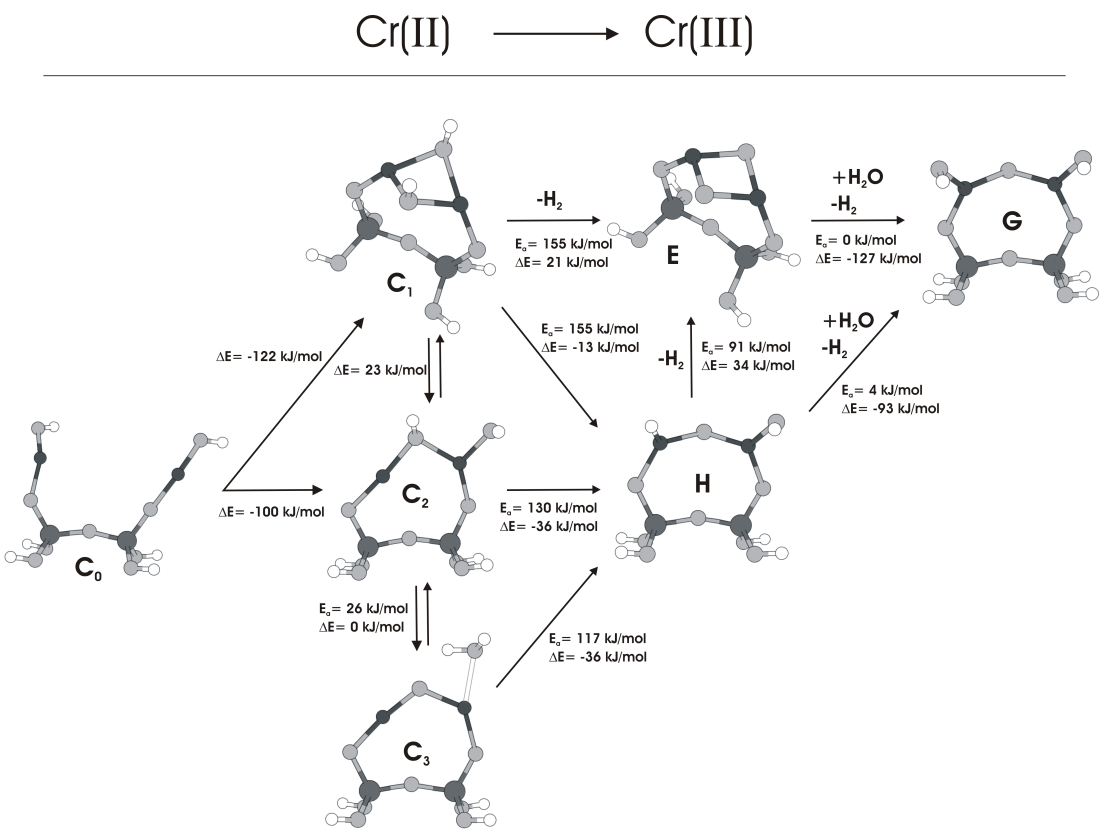

Figure 5.2: Optimized stationary structures on reaction paths leading to oxidation of two Cr(II) centers to Cr(III). For each reaction step in the figure, E_a represents the electronic activation energy and ΔE represents the change in electronic energy. (The figure is adapted from Fig. 3 of Paper III.)

values is associated with the specific siloxane structures involved in the translation of Cr(II) on silica as well as the limited size of the present cluster models.

5.2 Implications for Catalytically Active Cr(III)

As briefly described above, theoretical models have been obtained for the oxidation of Cr(II) to Cr(III) by water on amorphous silica. Moreover, based on the computations presented in Paper III and in Chapter 4 of this thesis summary, the product Cr(III) species, **E**, **H**, and **G** in Fig. 5.2 appear likely to catalyze dehydrogenation of ethane with a low barrier. These computational results are in agreement with experimental observations by DeRossi *et al.* [17]. There are, however, also some novel implications. As outlined above, the catalytically active species obtained by oxidation of Cr(II) by water appears to be the species known as redox Cr(III). It thus appears that redox Cr(III) is an oligomeric species even at low chromium load. Contrary to this, redox Cr(III) formed at low chromium load has been associated with mononuclear sites [3, 17, 19–21, 55],

A detailed discussion regarding the relationship between chromium nuclearity and oxidation state is given in Paper III. Briefly summarized, the presented computational results and experimental observations reported in the literature [32, 34, 52, 116, 117, 140] have the combined implication that redox Cr(III) on silica may form on sites of clustered Cr(III) oxide. This may take place either (i) through reduction of mononuclear Cr(VI) to mononuclear Cr(II) under formation of water, which causes subsequent aggregation of Cr(III) oxide, or (ii) through surface reduction of clusters already present on the calcined surface.

The implication that redox Cr(III) is a polynuclear structure may be taken one step further. With reports in the literature associating non-redox Cr(III) with clustered Cr(III) oxide [18, 22–25, 52], and now also redox Cr(III) being associated with clustered Cr(III) oxide, it may be proposed that the distinction of active Cr(III) in categories depending on redox history is an artifact of the approach of study, rather than there being an actual difference in structure.

5.3 Summary

Based on an experiment reported by DeRossi *et al.* [17] the oxidation of Cr(II) to Cr(III) by water on the surface of amorphous silica has been investigated by means of cluster models and density functional theory. The reaction is of interest since the product Cr(III) species, and the catalytically active species known as redox Cr(III), appear to be one and the same. Based on the computations, a reaction path appears viable which involves dimerization of Cr(II) prior to the oxidation step. This result is in line with a proposal by Groeneveld *et al.* [34] that hydrolysis of Cr(II)–OSi bonding leaves Cr(II) mobile on the silica surface. It appears that Cr(II)OH moieties are able to jump from one silicon tetrahedron to another in a mechanism involving rearrangement of siloxane rings. Subsequent oxidation to Cr(III) is found in the encounter between two Cr(II)OH moieties. The thermodynamic product of the reaction appears to be a dinuclear species of oxygen-linked Cr(III)OH centers. An implication of these computational results is that oligomer and even polymer Cr(III)/silica species may form in the reduction of mononuclear Cr(VI)/silica. This agrees with the observation that Cr(III) oxide aggregates during reduction with H_2 even on Cr/silica surfaces with chromium load below 1 wt% [34, 140]. Moreover, based on the computations presented in Paper III and in Chapter 4 of this thesis summary, the Cr(III) species obtained by oxidation of Cr(II) with water appear to catalyze dehydrogenation of ethane with a low barrier. This is in agreement with the report by DeRossi *et al.* [17], and the obtained Cr(III) structures thus appear as candidates for redox Cr(III). An implication of this results is that redox Cr(III) may be a structure of higher nuclearity than one even at low chromium load.

Chapter 6

Concluding Remarks

The general aim of this thesis has been to provide new foundation for extended understanding of the Cr/oxide catalysts for dehydrogenation of short alkanes. In particular, the aim has been to identify the chromium surface structures that contribute most efficiently, the mechanisms involved, and the role of the oxide support.

By means of density-functional theory and taking a cluster-model approach, we have investigated species of chromium(III) on alumina, silica, and chromia supports with respect to activity in catalytic dehydrogenation of ethane. Based on a proposal by DeRossi *et al.* [17] models have been prepared to represent variations of chromium(III) with three ligands covalently coordinated through oxygen. Furthermore, mechanisms of catalytic dehydrogenation have been constructed based on the assumption that the C–H activation step proceeds by σ-bond metathesis or by oxidative addition.

Based on the study of mononclear Cr(III)/silica, reported in Papers I and II, C–H activation by σ-bond metathesis appears as the favored route to catalytic dehydrogenation.

In Papers I and III, it was found that depending on the nano range surrounding the active site, the catalytic dehydrogenation of ethane may occur according to two different reaction paths. These mechanisms are characterized by the initial metathesis step involving a Cr–O bond or a Cr–H bond, and have been referred to as the σBM/CrO and σBM/CrH mechanism, respectively. The σBM/CrO mechanism consists of three elementary steps; (i) C–H/Cr–O activation by σ-bond metathesis gives an ethylchromium site and hydroxyl moiety in close interaction, (ii) transfer of a β-hydrogen from the ethyl ligand with immediate desorption of ethene renders a hydridochromium site, and (iii) the Cr–O bond is reforged in a σ-bond metathesis step which results in desorption of H_2. Apart from the absence of molecular adsorption of ethane, the mechanism is in agreement with a proposal in the literature [3]. The alternative σBM/CrH mechanism is based on a hydridochromium site as is formed in the second reaction step of the σBM/CrO mechanism. The catalytic cycle consists of two reaction steps; (i) C–H/Cr–H activation by σ-bond metathesis gives gaseous H_2 and an ethylchromium site, and (ii) the hydridochromium site is reformed by β-hydrogen transfer and desorption of ethene.

Based on free-energy calculations on models of structurally relaxed chromium species, the desorption of ethene appears rate determining for the σBM/CrO mechanism, while

the C–H activation step appears rate determining for the σBM/CrH mechanism. Furthermore, the relative strength of relaxed Cr–O and Cr–H bonds causes a significantly higher activation energy of the σBM/CrO mechanism compared to that of the σBM/CrH mechanism. The enthalpic barriers against dehydrogenation are obtained on the order of 100 and 200 kJ/mol, respectively.

Considering the computed activation energies, it appears that surface sites that are capable of stabilizing a reactive hydridochromium species are likely to contribute efficiently in catalytic dehydrogenation of ethane. However, to generate such a site an activation step appears necessary. Depending on the nano-range surroundings, chromium species with three covalently bonded oxygen ligands may be activated to accommodate the σBM/CrH mechanism through C–H activation by σ-bond metathesis involving a Cr–O bond. This reaction coincides with the initial C–H/Cr–O activation step of the σBM/CrO mechanism. However, the σBM/CrH mechanism owes its possible existence to the C–O cleavage being irreversible. Based on the computations in Papers I and III, a likely precursor to the active hydridochromium(III) species is a chromium(III)hydroxyl moiety bonded to the surface *via* two Cr–O–M linkages, M=Si, Al or Cr. On this species, water is formed by C–H/Cr–OH activation, and appears likely to desorb for entropic reasons. On the other hand, if the C–H activation reaction involves cleavage of a Cr–O–M linkage to the surface, a surface-bound hydroxyl is formed. Depending on the strain exerted by the surface, the hydroxyl may remain in close interaction with chromium, or relax away, thus making the Cr–O activation irreversible. In summary of Papers I and III, two-bridge CrOH species and strained three-bridge species appear as possible precursors to the catalytically active hydridochromium(III) site.

Computational results presented in this thesis summary indicate that dinuclear $Cr(\text{-}O\text{-})_2Cr$ species may be be active in catalytic dehydrogenation of ethane. The chromium centers in this structure are connected by two oxygen bridges, the chromium and oxygen atoms forming a strained four-membered ring. Due to structural relaxation upon ring opening in the C–H/Cr–O activation step, a relatively low activation barrier of around 130 kJ/mol is obtained for the σBM/CrO mechanism. However, the strain also gives rise to two extra reaction steps in the catalytic cycle; the hydroxyl moiety formed in the C–H activation step relaxes away from the active chromium center, and must subsequently rebound for reformation of the Cr–O bond to complete the catalytic cycle.

The role of the oxide support is addressed in Paper III. The choice of support being alumina, silica or chromia is concluded to have little effect on the energetics of the elementary reactions of the two catalytic cycles described above. Furthermore, structurally relaxed chromium(III) with three ligands covalently bonded through oxygen, appear too stable to be directly involved in the cycle of catalytic dehydrogenation. The role of the support is therefore suggested to be one of sustaining more reactive sites such as the hydridochromium species and the strained $Cr(\text{-}O\text{-})_2Cr$ species.

In a second approach to investigate the structure of active chromium(III), we have studied the oxidation by water of chromium(II) to chromium(III) on the surface of amorphous silica. This is the topic of Paper IV. The reaction is of interest since experiments indicate catalytic activity on the product Cr(III) species [17]. Based on the computations, hydrolysis of Cr–OSi bonding and travel of Cr(II)OH moieties across the silica surface

are suggested as important steps prior to to oxidation. The oxidation to chromium(III) is found in the encounter between two Cr(II)OH moieties. Dinuclear chromium(III) product species are thus obtained, reactive intermediates featuring hydridochromium(III) centers and a $Cr(\text{-}O\text{-})_2Cr$ ring structure, while the thermodynamic product in moist conditions is a species of Cr–O–Cr linked Cr(III)OH moieties. As summarized above, all these structures appear to catalyze dehydrogenation of ethane with a low barrier. Based on these computational results, Cr(III) oxide structures of nuclearity higher than one are proposed for the much discussed redox Cr(III) species.

Chapter 7

Suggestions for Further Work

The work of this thesis may be extended computationally as well as experimentally. With regard to further computations, there is a question of accuracy. The unpaired chromium *d* electrons pose a complex computational task to which multiconfiguration-wavefunction methods are suggested. In particular, this concerns the cases where redox processes are involved, such as when C–H activation takes place at a Cr–OCr bond, and when Cr(II) oxidates to Cr(III). Furthermore, the cluster models may be improved by embedding in the electrostatic field of the encapsulating surface.

Other improvements of the computational study pertain to the set of modelled structures and mechanisms. For instance, catalytic activity of Cr(II) has been proposed in the literature [16, 52], but remains an open question. In connection with the present thesis, preliminary investigation has been conducted of Cr(II)/silica with respect to catalytic dehydrogenation of ethane. Indications are obtained that C–H activation by σ-bond metathesis involving a Cr(II)–O bond leads to dehydrogenation with an activation barrier of around 200 kJ/mol, while hydridoCr(II) species appears too unstable to contribute. Furthermore, a mechanism based on C–H activation by oxidative addition appears interesting. However, there are issues of accuracy that must be resolved for that case.

Perhaps more interesting at this point than continuing the computational study, would be to explore experimentally the hypothesis that has been made based on the computations already performed. In the apparently most favorable mechanism of dehydrogenation, C–H activation proceeds by transfer of hydrogen to a chromium hydride. A hydrogen molecule is formed and ethyl ligates to chromium. The hydridochromium complex is then reformed by β-hydrogen transfer and desorption of ethene, i. e. the chromium hydride is reformed and a new cycle may follow. Thus, in the C–H activation step the hydrogen molecule is formed with hydrogen atoms from two different alkane molecules. This might be exploited in an isotope experiment using a reactant mixture of 50:50 C_nH_{2n+2} and C_nD_{2n+2}. If catalytic dehydrogenation is due mainly to C–H activation at a hydridochromium species, a H_2:HD:D_2 ratio close to 1:2:1 is to be expected. On the other hand, if dehydrogenation follows the alternative three-step mechanism involving activation and reformation of a Cr–O bond, no mixing is to be expected. Variations between the two extremes might indicate participation of both mechanisms. Consequently, mechanistic dependencies on catalyst composition and preparation may be addressed.

Bibliography

[1] Spitz, P. H. *Petrochemicals: The Rise of an Industry.* New York: Wiley, (1988).

[2] Arndtsen, B. A., Bergman, R. G., Mobley, T. A., and Peterson, T. H. *Acc. Chem. Res.* **28**, 154 (1995).

[3] Weckhuysen, B. M. and Schoonheydt, R. A. *Catal. Today* **51**, 223 (1999).

[4] Balat, M. and ozdemir, N. *Energy Source* **27**, 1285 (2005).

[5] Wittcoff, H. A. John Wiley & Sons, Inc., (2004).

[6] Hall, M. B. and Fan, H. J. *Adv. Inorg. Chem.* **54**, 321 (2003).

[7] Huff, M. and Schmidt, L. D. *J. Phys. Chem.* **97**, 815 (1993).

[8] Liebmann, L. S. and Schmidt, L. D. *Appl. Catal. A Gen.* **179**, 93 (1999).

[9] Beretta, A., Ranzi, E., and Forzatti, P. *Catal. Today* **64**, 103 (2001).

[10] Bhasin, M. M., McCain, J. H., Vora, B. V., Imai, T. T., and Pujadó, P. R. *Appl. Catal. A Gen.* **221**, 397 (2001).

[11] Frey, F. E. and Huppke, W. F. *Ind. Eng. Chem.* **25**, 54 (1933).

[12] Poole, C. P. and Maciver, D. S. *Adv. Catal.* **17**, 223 (1967).

[13] Craig, R. G. and Dufallo, J. M. *Chem. Eng. Prog.* **75**, 62 (1979).

[14] König, P. and Tétényi, P. *Acta Chim. Hung.* **89**, 123 (1976).

[15] König, P. and Tétényi, P. *Acta Chim. Hung.* **89**, 137 (1976).

[16] Lugo, H. I. and Lunsford, J. H. *J. Catal.* **91**, 155 (1985).

[17] DeRossi, S., Ferraris, G., Fremiotti, S., Garrone, E., Ghiotti, G., Campa, M. C., and Indovina, V. *J. Catal.* **148**, 36 (1994).

[18] Cavani, F., Koutyrev, M., Trifirò, F., Bartolini, A., Ghisletti, D., Iezzi, R., Santucci, A., and Piero, G. D. *J. Catal.* **158**, 236 (1996).

[19] DeRossi, S., Ferraris, G., Fremiotti, S., Indovina, V., and Cimino, A. *Appl. Catal. A Gen.* **106**, 125 (1993).

[20] DeRossi, S., Casaletto, M. P., Ferraris, G., Cimino, A., and Minelli, G. *Appl. Catal. A Gen.* **167**, 257 (1998).

[21] Hakuli, A., Kytökivi, A., Krause, A. O. I., and Suntola, T. *J. Catal.* **161**, 393 (1996).

[22] Hakuli, A., Kytökivi, A., and Krause, A. O. I. *Appl. Catal. A Gen.* **190**, 219 (2000).

[23] Airaksinen, S. M. K., Kanervo, J. M., and Krause, A. O. I. *Stud. Surf. Sci. Catal.* **136**, 153 (2001).

[24] Puurunen, R. L. and Weckhuysen, B. M. *J. Catal.* **210**, 418 (2002).

[25] Puurunen, R. L., Airaksinen, S. M. K., and Krause, A. O. I. *J. Catal.* **213**, 281 (2003).

[26] Weckhuysen, B. M., Bensalem, A., and Schoonheydt, R. A. *J. Chem. Soc., Faraday Trans.* **94**, 2011 (1998).

[27] Gaspar, A. B., Brito, J. L. F., and Dieguez, L. C. *J. Mol. Catal. A* **203**, 251 (2003).

[28] Gaspar, A. B. and Dieguez, L. C. *J. Catal.* **220**, 309 (2003).

[29] Duffy, J. A. *Bonding, Energy levels and Bands.* Longman Scientific & Technical, (1990).

[30] Fouad, N. E., Knözinger, H., Zaki, M. I., and Mansour, S. A. A. *Z. Phys. Chem.* **171**, 75 (1991).

[31] Weckhuysen, B. M., DeRidder, L. M., Grobet, P. J., and Schoonheydt, R. A. *J. Phys. Chem.* **99**, 320 (1995).

[32] Weckhuysen, B. M., DeRidder, L. M., and Schoonheydt, R. A. *J. Phys. Chem.* **97**, 4756 (1993).

[33] Airaksinen, S. M. K., Krause, A. O. I., Sainio, H., Lahtinen, J., Chao, K.-J., Guerroro-Pérez, M. L., and Banãres, M. A. *Phys. Chem. Chem. Phys.* **5**, 4371 (2003).

[34] Groeneveld, C., Wittgen, P. P. M. M., Vankersbergen, A. M., Mestrom, P. L. M., Nuijten, C. E., and Schuit, G. C. A. *J. Catal.* **59**, 153 (1979).

[35] Weckhuysen, B. M., Wachs, I. E., and Schoonheydt, R. A. *Chem. Rev.* **96**, 3327 (1996).

[36] McDaniel, M. P. *J. Catal.* **76**, 37 (1982).

[37] Hardcastle, F. D. and Wachs, I. E. *J. Mol. Catal.* **46**, 173 (1988).

[38] Vuurman, M. A., Hardcastle, F. D., and Wachs, I. E. *J. Mol. Catal.* **84**, 193 (1993).

[39] Vuurman, M. A., Wachs, I. E., Stufkens, D. J., and Oskam, A. *J. Mol. Catal.* **80**, 209 (1993).

[40] Mentasty, L. R., Gorriz, O. F., and Cadús, L. E. *Ind. Eng. Chem. Res.* **38**, 396 (1999).

[41] McDaniel, M. P. *J. Catal.* **76**, 17 (1982).

[42] Kim, D. S., Tatibouet, J.-M., and Wachs, I. E. *J. Catal.* **136**, 209 (1992).

[43] Haukka, S., Lakomaa, E.-L., and Suntola, T. *Appl. Surf. Sci.* **75**, 220 (1994).

[44] Liu, B. and Terano, M. *J. Mol. Catal. A* **172**, 227 (2001).

[45] Grünert, W., Saffert, W., Feldhaus, R., and Anders, K. *J. Catal.* **99**, 149 (1986).

[46] Grünert, W., Shipiro, E. S., Feldhaus, R., Anders, K., Antoshin, G. V., and Minachev, K. M. *J. Catal.* **100**, 138 (1986).

[47] Airaksinen, S. M. K., Harlin, M. E., and Krause, A. O. I. *Ind. Eng. Chem. Res.* **41**, 5619 (2002).

[48] Airaksinen, S. M. K. and Krause, A. O. I. *Ind. Eng. Chem. Res.* **44**, 3862 (2005).

[49] Kim, D. S. and Wachs, I. E. *J. Catal.* **142**, 166 (1993).

[50] Ashmawy, F. M. *J. Chem. Soc., Faraday Trans. I* **76**, 2096 (1980).

[51] Marcilly, C. and Delmon, B. *J. Catal.* **24**, 336 (1972).

[52] Hakuli, A., Harlin, M. E., Backman, L. B., and Krause, A. O. I. *J. Catal.* **184**, 349 (1999).

[53] Weckhuysen, B. M., Verberckmoes, A. A., Debaere, J., Ooms, K., Langhans, I., and Schoonheydt, R. A. *J. Mol. Catal. A* **151**, 115 (2000).

[54] DeRossi, S., Ferraris, G., Fremiotti, S., Cimino, A., and Indovina, V. *Appl. Catal. A* **81**, 113 (1992).

[55] Kytökivi, A., Jacobs, J. P., Hakuli, A., Merilainen, J., and Brongersma, H. H. *J. Catal.* **162**, 190 (1996).

[56] Masson, J., Bonnier, J. M., Duvigneaud, P. H., and Delmon, B. *J. Chem. Soc., Faraday Trans. I* **73**, 1471 (1977).

[57] Gorriz, O. F., Corberán, V. C., and Fierro, J. L. G. *Ind. Eng. Chem. Res.* **31**, 2670 (1992).

[58] Ghiotti, G. and Chiorino, A. *Spectrochim. Acta A* **49**, 1345 (1993).

[59] Olsbye, U., Virnovskaia, A., Prytz, O., Tinnemans, S. J., and Weckhuysen, B. M. *Catal. Lett.* **103**, 143 (2005).

[60] Sauer, J., Ugliengo, P., Garrone, E., and Saunders, V. R. *Chem. Rev.* **94**, 2095 (1994).

[61] Sauer, J. and Sierka, M. *J. Comput. Chem.* **21**, 1470 (2000).

[62] Lin, H. and Truhlar, D. G. *J. Phys. Chem. A* **109**, 3991 (2005).

[63] Kubicki, J. D. and Apitz, S. E. *Am. Mineral.* **83**, 1054 (1998).

[64] Handzlik, J. and Ogonowski, J. *J. Mol Catal. A-Chem.* **175**, 215 (2001).

[65] Vito, D. A. D., Gilardoni, F., Kiwi-Minsker, L., Morgantini, P.-Y., Porchet, S., Renken, A., and Weber, J. *THEOCHEM* **469**, 7 (1999).

[66] Børve, K. J. and Espelid, Ø. In *Nanostructured Catalysts,* Scott, S. L., Crudden, C. M., and Jones, C. W., editors, volume 3 of *Nanostructure science and technology*, 85. Kluwer Academic, New York (2002).

[67] Bray, M. R., Deeth, R. J., and Paget, V. J. *Prog. React. Kinet.* **21**, 169 (1996).

[68] Cramer, C. J. Wiley, (2002).

[69] Jensen, F. Wiley, (1999).

[70] Born, M. and Oppenheimer, R. *Ann. Phys.* **84**, 457 (1927).

[71] Slater, J. C. *Phys. Rev.* **35**, 210 (1930).

[72] Hartree, D. R. *Proc. Camb. Phil. Soc.* **24**, 328 (1928).

[73] Fock, V. A. *Z. Phys.* **15**, 126 (1928).

[74] Roothan, C. C. *Rev. Mod. Phys.* **23**, 69 (1951).

[75] Hall, G. G. *Proc. R. Soc. London, Ser. A* **205**, 541 (1951).

[76] Roos, B. In *Advances in Chemical Physics,* Lawley, K., editor, volume 69, 339. Wiley Interscience, New York (2002).

[77] Møller, C. and Plesset, M. S. *Phys. Rev.* **46**, 618 (1934).

[78] Roos, B. O., Andersson, K., Fulscher, M. K., Malmqvist, P.-A., Serrano-Andres, L., Pierloot, K., and Merchan, M. *Adv. Chem. Phys.* **93**, 219 (1996).

[79] Nakano, H. *J. Chem. Phys.* **99**, 7983 (1993).

[80] Hohenberg, P. and Kohn, W. *Phys. Rev. B* **136**, 864 (1964).

[81] Kohn, W. and Sham, L. *Phys. Rev. A* **140**, 1133 (1965).

[82] Gunnarsson, O. and Lundquist, I. *Phys. Rev. B* **13**, 4274 (1928).

[83] von Barth, U. and Hedin, L. *Phys. Rev. A* **20**, 1693 (1979).

[84] Alder, D. M. C. B. J. *Phys. Rev. Lett.* **45**, 566 (1980).

[85] Vosko, S. H., Wilk, L., and Nusair, M. *Can. J. Phys.* **58**, 1200 (1980).

[86] Slater, J. C. *The Self-Consistent Field for Molecular and Solids*, volume 4. McGraw-Hill, New York, (1974).

[87] Becke, A. D. *Phys. Rev. A* **38**, 3098 (1988).

[88] Perdew, J. P. *Phys. Rev. B* **33**, 8822 (1986).

[89] Stevens, P. J., Devlin, F. J., Chablowski, C. F., and Frisch, M. J. *J. Phys. Chem.* **98**, 11623 (1994).

[90] Friesner, R. A. *PNAS* **102**, 6648 (2005).

[91] SQ, S. Q. N. and Hall, M. B. *Chem. Rev.* **100**, 353 (2000).

[92] Gale, J. D. *J. Chem. Soc., Faraday Trans.* **93**, 629 (1997).

[93] Gale, J. D. *Phil. Mag. B* **73**, 3 (1996).

[94] Gale, J. D. and Rohl, A. L. *Mol. Simul.* **29**, 291 (2003).

[95] Ferré, N., Assfeld, X., and Rivail, J. L. *J. Comput. Chem.* **23**, 610 (2002).

[96] Monard, G., Loos, M., Thery, V., Baka, K., and Rivail, J. L. *Int. J. Quantum Chem.* **58**, 153 (1996).

[97] Sierka, M. and Sauer, J. *J. Phys. Chem.* **112**, 6983 (2000).

[98] Baerends, E. J., Autschbach, J. A., Bérces, A., Bo, C., Boerrigter, P. M., Cavallo, L., Chong, D. P., Deng, L., Dickson, R. M., Ellis, D. E., Fan, L., Fischer, T. H., Fonseca Guerra, C., van Gisbergen, S. J. A., Groeneveld, J. A., Gritsenko, O. V., Grüning, M., Harris, F. E., van den Hoek, P., Jacobsen, H., van Kessel, G., Kootstra, F., van Lenthe, E., Osinga, V. P., Patchkovskii, S., Philipsen, P. H. T., Post, D., Pye, C. C., Ravenek, W., Ros, P., Schipper, P. R. T., Schreckenbach, G., Snijders, J. G., Sola, M., Swart, M., Swerhone, D., te Velde, G., Vernooijs, P., Versluis, L., Visser, O., van Wezenbeek, E., Wiesenekker, G., Wolff, S. K., Woo, T. K., , and Ziegler, T. *ADF 2002.03 Computer Code*, (2002).

[99] Schröder, D., Shaik, S., and Schwarz, H. *Acc. Chem. Res.* **33**, 139 (2000).

[100] Harvey, J. N., Poli, R., and Smith, K. M. *Coord. Chem. Rev.* **238**, 347 (2003).

[101] Harvey, J. N., Aschi, M., Schwarz, H., and Koch, W. *Theor. Chem. Acc.* **99**, 95 (1998).

[102] Harvey, J. N. and Aschi, M. *Phys. Chem. Chem. Phys.* **1**, 5555 (1999).

[103] Jensen, V. R. and Børve, K. J. *Organometallics* **16**, 2514 (1997).

[104] Jensen, V. R. and Børve, K. J. *J. Comp. Chem.* **19**, 947 (1998).

[105] Ziegler, T. *Chem. Rev.* **91**, 651 (1991).

[106] Ziegler, T. *Can. J. Chem.* **73**, 743 (1995).

[107] Harvey, J. N. *Struct. Bond* **112**, 151 (2004).

[108] Poli, R. and Harvey, J. N. *Chem. Soc. Rev.* **32**, 1 (2003).

[109] Raybaud, P., Digne, M., Iftimie, R., Wellens, W., Euzen, P., and Toulhoat, H. *J. Catal.* **201**, 236 (2001).

[110] Groeneveld, C., Wittgen, P. P. M. M., Swinnen, H. P. M., Wernsen, A., and Schuit, G. C. A. *J. Catal.* **83**, 346 (1983).

[111] Wittgen, P. P. M. M., Groeneveld, C., Zwaans, P. J. C. J. M., Morgenstern, H. J. B., Vanheughten, A. H., Vanheumen, C. H. M., and Schuit, G. C. A. *J. Catal.* **77**, 360 (1982).

[112] Wittgen, P. P. M. M., Groeneveld, C., J. H. G. J. Janssens, M. L. J. A. W., and Schuit, G. C. A. *J. Catal.* **59**, 168 (1979).

[113] Limoge, Y. *Cr. Acad. Sci. IV-Phys.* **2**, 263 (2001).

[114] Zecchina, A., Garrone, E., Ghiotti, G., Morterra, C., and Borello, E. *J. Phys. Chem.* **79**, 966 (1975).

[115] Kim, C. S. and Woo, S. I. *J. Mol. Catal.* **73**, 249 (1992).

[116] Groppo, E., Lamberti, C., Bordiga, S., Spoto, G., and Zecchina, A. *Chem. Rev.* **105**, 115 (2005).

[117] Groppo, E., Damin, A., Bonino, F., Bordiga, S., Zecchina, A., and Lamberti, C. *Chem. Mater.* **17**, 2019 (2005).

[118] Burwell, R. L., Littlewood, A. B., Cardew, M., Pass, G., and Stoddard, C. T. H. *J. Am. Chem. Soc.* **82**, 6272 (1960).

[119] Stahl, S. S., Labinger, J. A., and Bercaw, J. E. *Angew. Chem. Int. Ed.* **37**, 2181 (1998).

[120] Siegbahn, P. E. M. and Crabtree, R. H. *J. Am. Chem. Soc.* **118**, 4442 (1996).

[121] Casty, G. L., Matturro, M. G., Myers, G. R., Reynolds, R. P., and Hall, R. P. *Organometallics* **20**, 2246 (2001).

[122] Milet, A., Dedieu, A., Kapteijn, G., and van Koten, G. *Inorg. Chem.* **36**, 3223 (1997).

[123] Whittlesey, M. K., Mawby, R. J., Osman, R., Perutz, R. N., Field, L. D., Wilkinson, M. P., and George, M. W. *J. Am. Chem. Soc.* **115**, 8627 (1993).

[124] Xu, X., Faglioni, F., and W. A. Goddard, III. *J. Phys. Chem. A* **106**, 7171 (2002).

[125] Filippou, A. C., Schneider, S., and Schnakenburg, G. *Angew. Chem. Int. Ed.* **42**, 4486 (2003).

[126] Shapovalov, V. and Truong, T. N. *J. Phys. Chem. B* **104**, 9859 (2000).

[127] Wittbrodt, J. M., Hase, W. L., and Schlegel, H. B. *J. Phys. Chem. B* **102**, 6539 (1998).

[128] Schmidt, M. W., Baldridge, K. K., Boatz, J. A., Elbert, S. T., Gordon, M. S., Jensen, J. H., Koseki, S., Matsunaga, N., Nguyen, K. A., Su, S., Windus, T. L., Dupuis, M., and Montgomery, J. A. *J. Comput. Chem.* **14**, 1347 (1993).

[129] Frisch, M. J., Trucks, G. W., Schlegel, H. B., Scuseria, G. E., Robb, M. A., Cheeseman, J. R., Montgomery, Jr., J. A., Vreven, T., Kudin, K. N., Burant, J. C., Millam, J. M., Iyengar, S. S., Tomasi, J., Barone, V., Mennucci, B., Cossi, M., Scalmani, G., Rega, N., Petersson, G. A., Nakatsuji, H., Hada, M., Ehara, M., Toyota, K., Fukuda, R., Hasegawa, J., Ishida, M., Nakajima, T., Honda, Y., Kitao, O., Nakai, H., Klene, M., Li, X., Knox, J. E., Hratchian, H. P., Cross, J. B., Bakken, V., Adamo, C., Jaramillo, J., Gomperts, R., Stratmann, R. E., Yazyev, O., Austin, A. J., Cammi, R., Pomelli, C., Ochterski, J. W., Ayala, P. Y., Morokuma, K., Voth, G. A., Salvador, P., Dannenberg, J. J., Zakrzewski, V. G., Dapprich, S., Daniels, A. D., Strain, M. C., Farkas, O., Malick, D. K., Rabuck, A. D., Raghavachari, K., Foresman, J. B., Ortiz, J. V., Cui, Q., Baboul, A. G., Clifford, S., Cioslowski, J., Stefanov, B. B., Liu, G., Liashenko, A., Piskorz, P., Komaromi, I., Martin, R. L., Fox, D. J., Keith, T., Al-Laham, M. A., Peng, C. Y., Nanayakkara, A., Challacombe, M., Gill, P. M. W., Johnson, B., Chen, W., Wong, M. W., Gonzalez, C., and Pople, J. A.

[130] Espelid, Ø. and Børve, K. J. *J. Phys. Chem. A* **102**, 9449 (1997).

[131] Busca, G. *J. Catal.* **120**, 303 (1989).

[132] Vidal, V., Théolier, A., Thivolle-Cazat, J., and Basset, J.-M. *Science* **276**, 99 (1997).

[133] Maury, O., Lefort, L., Vidal, V., Thivolle-Cazat, J., and Basset, J.-M. *Angew. Chem. Int. Ed.* **38**, 1952 (1999).

[134] Mikhailov, M. N., Bagaturi´yants, A. A., and Kustov, L. M. *Russ. Chem. Bull. Int. Ed.* **52**, 30 (2003).

[135] Kao, J.-Y., Piet-Lahanier, H., Walter, E., and Happel, J. *J. Catal.* **133**, 383 (1992).

[136] Indovina, V., Cimino, A., DeRossi, S., Ferraris, G., Ghiotti, G., and Chiorino, A. *J. Mol. Catal.* **75**, 305 (1992).

[137] Nijhuis, T. A., Tinnemans, S. J., Visser, T., and Weckhuysen, B. M. *Phys. Chem. Chem. Phys.* **5**, 4361 (2003).

[138] Nijhuis, T. A., Tinnemans, S. J., Visser, T., and Weckhuysen, B. M. *Chem. Eng. Sci.* **59**, 5487 (2004).

[139] Weckhuysen, B. M., Verberckmoes, A. A., Buttiens, A. L., and Schoonheydt, R. A. *J. Phys. Chem.* **98**, 579 (1994).

[140] Liotta, L. F., Venezia, A. M., Panteleo, G., Deganello, G., Gruttadauria, M., and Noto, R. *Catal. Today* **91**, 843 (1993).